BRAIN
ORIGINAL ARTICLE

Lewy pathology formation in patient-derived *GBA1* Parkinson's disease midbrain organoids

Emanuele Frattini,[1] Gaia Faustini,[2] Gianluca Lopez,[3] Emma Veronica Carsana,[4] Mattia Tosi,[1] Ilaria Trezzi,[1] Manuela Magni,[1] Giulia Soldà,[5,6] Letizia Straniero,[5,6] Daniele Facchi,[5,6] Maura Samarani,[7] Mitchell Martá-Ariza,[8,9] Chiara Maria Giulia De Luca,[10] Elena Vezzoli,[11] Alessandra Pittaro,[3] Astghik Stepanyan,[12] Rosamaria Silipigni,[13] Isabel Rosety,[14] Jens C. Schwamborn,[14] Sergio Pablo Sardi,[15] Fabio Moda,[10] Stefania Corti,[1,16] Giacomo P. Comi,[1,16] Fabio Blandini,[17] Nicolas X. Tritsch,[18,19,†] Mario Bortolozzi,[20,21] Stefano Ferrero,[3,22] Fulvia Milena Cribiù,[3,‡] Thomas Wisniewski,[8,23,24] Rosanna Asselta,[5,6] Massimo Aureli,[4] Arianna Bellucci[2] and Alessio Di Fonzo[1]

Fibrillary aggregation of α-synuclein in Lewy body inclusions and nigrostriatal dopaminergic neuron degeneration define Parkinson's disease neuropathology. Mutations in *GBA1*, encoding glucocerebrosidase, are the most frequent genetic risk factor for Parkinson's disease. However, the lack of reliable experimental models able to reproduce key neuropathological signatures has hampered clarification of the link between mutant glucocerebrosidase and Parkinson's disease pathology.

Here, we describe an innovative protocol for the generation of human induced pluripotent stem cell-derived midbrain organoids containing dopaminergic neurons with nigral identity that reproduce characteristics of advanced maturation. When applied to patients with *GBA1*-related Parkinson's disease, this method enabled the differentiation of midbrain organoids recapitulating dopaminergic neuron loss and fundamental features of Lewy pathology observed in human brains, including the generation of α-synuclein fibrillary aggregates with seeding activity that also propagate pathology in healthy control organoids. Concurrently, we found that the retention of mutant glucocerebrosidase in the endoplasmic reticulum and increased levels of its substrate, glucosylceramide, are determinants of α-synuclein aggregation into Lewy body-like inclusions, and the reduction of glucocerebrosidase activity accelerated α-synuclein pathology by promoting fibrillary α-synuclein deposition.

Finally, we demonstrated the efficacy of ambroxol and GZ667161 (two modulators of the glucocerebrosidase pathway in clinical development for the treatment of *GBA1*-related Parkinson's disease) in reducing α-synuclein pathology in this model, supporting the use of midbrain organoids as a relevant preclinical platform for investigational drug screening.

1 Neurology Unit, IRCCS Foundation Ca' Granda Ospedale Maggiore Policlinico, Milan 20122, Italy
2 Department of Molecular and Translational Medicine, University of Brescia, Brescia 25123, Italy
3 Division of Pathology, IRCCS Foundation Ca' Granda Ospedale Maggiore Policlinico, University of Milan, Milan 20122, Italy
4 Department of Medical Biotechnology and Translational Medicine, University of Milano, Milan 20054, Italy
5 Department of Biomedical Sciences, Humanitas University, Pieve Emanuele, Milan 20072, Italy

Received November 27, 2023. Revised September 13, 2024. Accepted October 01, 2024. Advance access publication November 21, 2024

6 Medical Genetics and RNA Biology Unit, IRCCS Humanitas Research Hospital, Rozzano, Milan 20089, Italy
7 Unité de Trafic Membranaire et Pathogénèse, Département de Biologie Cellulaire et de l'Infection, Institut Pasteur, Paris 75015, France
8 Center for Cognitive Neurology, Department of Neurology, New York University Grossman School of Medicine, New York, NY 10016, USA
9 Institut de Neurociències, Universitat Autònoma de Barcelona, Barcelona 08193, Spain
10 Division of Neurology 5 and Neuropathology, Fondazione IRCCS Istituto Neurologico Carlo Besta, Milan 20133, Italy
11 Advanced Light and Electron Microscopy BioImaging Centre (ALEMBIC), IRCCS San Raffaele Scientific Institute, Milan 20132, Italy
12 Unità Operativa Complessa, Chirurgia Generale 3, University Hospital of Padua, Padua 35128, Italy
13 Laboratory of Medical Genetics, IRCCS Foundation Ca' Granda Ospedale Maggiore Policlinico, Milan 20122, Italy
14 Luxembourg Centre for Systems Biomedicine (LCSB), Developmental and Cellular Biology, University of Luxembourg, Belvaux L-4367, Luxembourg
15 Rare and Neurological Diseases Therapeutic Area, Sanofi, Framingham, MA 01701, USA
16 Department of Pathophysiology and Transplantation (DEPT), Dino Ferrari Centre, University of Milan, Milan 20122, Italy
17 Foundation IRCCS Ca' Granda Ospedale Maggiore Policlinico, Milan 20122, Italy
18 Neuroscience Institute, New York University Grossman School of Medicine, New York, NY 10016, USA
19 Fresco Institute for Parkinson's and Movement Disorders, New York University Langone Health, New York, NY 10017, USA
20 Department of Physics and Astronomy 'G. Galilei', University of Padua, Padua 35131, Italy
21 Veneto Institute of Molecular Medicine (VIMM), Padua 35129, Italy
22 Department of Biomedical, Surgical, and Dental Sciences, University of Milan, Milan 20122, Italy
23 Department of Pathology, New York University Grossman School of Medicine, New York, NY 10016, USA
24 Department of Psychiatry, New York University Grossman School of Medicine, New York, NY 10016, USA

† Present address: Douglas Hospital Research Center, McGill University, Montreal, QC H4H 1R3, Canada
‡ Present address: SC Anatomia e Istologia Patologica, Ospedale di Treviglio-Caravaggio-Ospedale di Romano di Lombardia ASST BG Ovest, Italy

Correspondence to: Alessio Di Fonzo, MD, PhD,
Neurology Unit, IRCCS Foundation Ca' Granda Ospedale Maggiore Policlinico
Via Francesco Sforza 35, Milan 20122, Italy
E-mail: alessio.difonzo@policlinico.mi.it

Correspondence may also be addressed to: Emanuele Frattini, MD, PhD
E-mail: emanuele.frattini@policlinico.mi.it; emanuele.frattini@gmail.com

Keywords: Parkinson's disease; midbrain organoids; Lewy bodies; *GBA1*; glucocerebrosidase; ambroxol

Introduction

Parkinson's disease (PD), caused predominantly by the degeneration of dopaminergic (DA) neurons in the midbrain substantia nigra (SN), is the most common neurodegenerative movement disorder[1] and an emerging public health concern in the ageing population.[2] Lewy bodies (LBs) and Lewy neurites (LNs), insoluble inclusions affecting the cytoplasm and processes of neuronal cells, are defining neuropathological hallmarks of PD.[3] A heterogeneous mixture of proteins, membranes and lipids accumulates in LB deposits, with α-synuclein (α-syn) fibrils being the major component.[4-6]

Mutations in *GBA1* (e.g. L444P), encoding the lysosomal glucosylceramide (GlcCer)-catalysing enzyme glucocerebrosidase (GCase), are the most frequent genetic risk factor for PD.[7] GCase insufficiency owing to biallelic *GBA1* mutations leads to cellular accumulation of GlcCer and causes Gaucher's disease (GD).[8] Interestingly, GD patients have a similar increased risk of developing PD to monoallelic *GBA1* mutation carriers.[9] Compelling evidence supports that mutant GCase misfolding and enzymatic deficiency, along with accumulation of glycosphingolipid substrates, drive α-syn aggregation in *GBA1*-related PD.[10-13] This notwithstanding, whether and how the impaired GCase pathway can induce α-syn pathological deposition and neuronal degeneration in PD remains to be determined. A main obstacle in this endeavour is the lack of reliable models able to recapitulate *GBA1*-PD neuropathology faithfully.

Here, we describe an innovative approach for the generation of human induced pluripotent stem cell (iPSC)-derived midbrain organoids (MOs) that contain mature DA neurons exhibiting key nigrostriatal-like characteristics and abundant neuromelanin pigmentation. This method was used to investigate the link between mutant GCase and α-syn pathology in MOs from *GBA1*-PD patients. We found that *GBA1*-PD MOs present DA neurodegeneration and develop α-syn deposits recapitulating the major defining biochemical, immunohistochemical, ultrastructural and morphological features of Lewy pathology observed in the brains of PD patients. Notably, these included efficient α-syn seeding activity as demonstrated by seed amplification assay and by the propagation of α-syn fibrillary aggregates in healthy control MOs inoculated with insoluble protein extracts derived from *GBA1*-PD MOs. Remarkably, we also found that the retention of mutant GCase in

the endoplasmic reticulum (ER) and the increase of GlcCer resulting from impaired GCase activity are key drivers of α-syn pathology. Finally, we demonstrated that ambroxol and GZ667161, two modulators of the GCase pathway in clinical development for the treatment of *GBA1*-related PD, reduce LB-like fibrillary α-syn deposition in patient-derived MOs, thus validating our model as a valuable preclinical tool for drug screening.

Materials and methods

Human samples

IPSC lines were generated from fibroblasts of one PD patient carrying the *GBA1* L444P heterozygous mutation (PD^{L444P}), one patient affected by both GD and PD carrying the *GBA1* L444P homozygous mutation (GD/PD^{L444P}) and two age- and sex-matched healthy donors with wild-type *GBA1* ($CTR1^{wt}$ and $CTR2^{wt}$). One additional control iPSC line ($CTR3^{wt}$) was purchased from the ATCC cell bank (#ACS-1023; American Type Culture Collection).

Paraffin-embedded sections and fresh frozen tissue collected from the SN pars compacta of the PD^{L444P} patient (SNc_PD^{L444P}) and from three healthy donors (SNc_CTR1^{wt}, SNc_CTR2^{wt} and SNc_CTR3^{wt}), kindly supplied by the Parkinson's UK Brain Bank and used by Longhena *et al.*,[14] were used for immunostaining and biochemical analyses. Brain homogenates from three patients with PD (PD#1, PD#2 and PD#3) and two patients with multiple system atrophy type-P (MSA#1 and MSA#2) were used for α-syn seed amplification assay.

The demographic data of donors of samples used in the study are illustrated in Supplementary Table 1 and discussed in the Supplementary material, 'Clinical data' section. Additional details can be found in the Supplementary material, 'Methods' section.

Generation of midbrain organoids

IPSC lines were differentiated into MOs with a novel DA-patterning protocol adapted from Lancaster *et al.*[15] and Kriks *et al.*[16] On Day 0, iPSCs were aggregated into embryoid bodies in 96-well ultra-low-attachment plates and cultured in hES medium [Dulbecco's modified Eagle medium (DMEM)/F12, 20% KnockOut Serum Replacement (KSR), 3% fetal bovine serum (FBS), 1% GlutaMax, 1% Minimum Essential Medium Non-Essential Amino Acids (MEM-NEAA)] for 6 days. Embryoid bodies were subsequently transferred to 24-well ultra-low-attachment plates and subdued to neural induction in a minimal medium (DMEM/F12, 1% N2 supplement, 1% GlutaMax, 1% MEM-NEAA) for another 4 days. On Day 11, tissues were embedded into Cultrex (R&D) and cultured in cerebral organoid medium (48% DMEM/F12, 48% Neurobasal, 0.5% N2 supplement, 0.4 μM insulin, 1% GlutaMax, 0.5% MEM-NEAA, 1% penicillin/streptomycin stock solution, 48 μM 2-mercaptoethanol and 1% B27 supplement without vitamin A) for 4 days. On Day 14, organoids were transferred to spinning bioreactors (Corning) and cultured for up to 150 days. In the spinner flask, MOs were cultured for 11 days in KSR medium (DMEM, 15% KSR, 1% MEM-NEAA, 1% penicillin/streptomycin stock solution and 10 μM 2-mercaptoethanol) and N2 medium (DMEM, 1% N2 supplement and 1% penicillin/streptomycin stock solution) supplemented with 10 μM SB431542 (Days 14–18), 100 nM LDN193189 (Days 14–24), 2 μM purmorphamine (Days 15–20), 250 nM SAG (Days 15–20), 50 ng/ml FGF8b (Days 15–20) and 3 μM CHIR99021 (Days 17–26). Following DA induction, MOs were maintained in B27 medium (Neurobasal, 2% B27 supplement, 1% GlutaMax and 1% penicillin/streptomycin stock solution) supplemented with BDNF 10 ng/ml, 10 ng/ml GDNF, 1 ng/ml TFGb3, 100 μM dibutyryl-cAMP and 200 μM ascorbic acid.

Double 3D immunofluorescence staining of clarified whole midbrain organoids

MOs at 50, 100 and 150 days *in vitro* (DIV) were fixed for 1 h at room temperature in Immunofix and washed three times with 0.1 M PBS. Fixed MOs were permeabilized for 2 h in 0.1 M PBS supplemented with 20% methanol and 0.1% Triton X-100, washed and incubated overnight at room temperature in blocking solution (10% normal goat serum, 0.1% Triton X-100 in 0.1 M PBS), then with primary antibodies at proper dilution (Supplementary Table 2) in blocking solution for 5 days at room temperature. MOs were washed three times with 0.1% Triton X-100 in 0.1 M PBS for 24 h and incubated with the fluorochrome-conjugated secondary antibodies (goat anti-mouse cy3 and goat anti-rabbit Alexa Fluor 488, Jackson Immunoresearch) in 0.1% Triton X-100 in 0.1 M PBS plus 3% normal goat serum for 5 days at room temperature. After three washes in 0.1% Triton X-100 in PBS for 24 h, cells were clarified overnight in 47% 2,2′-thiodiethanol (TDE) and observed by means of a Zeiss confocal laser microscope LSM 880 with tile scan and z-stack reconstructions. Images (512 × 512 pixels) were then reconstructed using Zen lite 2.3.

Immunohistochemistry of proteinase K-resistant α-synuclein in midbrain organoids and human brains

Proteinase K (PK)-resistant α-syn was visualized by chromogenic and fluorescent immunohistochemistry (IHC) using our previously described protocols.[17,18] Briefly, 8-μm-thick sections from MOs and from the SN of the *GBA1*-PD donor patient of the PD^{L444P} iPSC line (SNc_PD^{L444P}) were deparaffinized and rehydrated through a series of xylene and ethanol washes. Sections were incubated with a working solution of PK (1:500; Enzo Life Sciences, Cat. No. ENZ-33801) for 20 min at 37°C. Further antigen retrieval was performed by treatment with 88% formic acid for 7 min, followed by boiling in citrate buffer (10 mM sodium citrate and 0.05% Tween-20; pH 6). For chromogenic IHC only, endogenous peroxidase activity was blocked using 0.3% H_2O_2 for 20 min. Sections were blocked with 10% normal goat serum and incubated overnight at 4°C with either one of two anti-aggregated α-syn primary antibodies (BioLegend, Cat. No. 847902, 1:100; BioLegend, Cat. No. 824301, 1:200). For fluorescent IHC, sections were incubated with an anti-mouse IgG fluorescent or biotinylated secondary antibody (1:500, from Jackson ImmunoResearch, 2 h at room temperature; or 1:1000, from Vector Labs, 1 h at room temperature). For chromogenic IHC, sections were incubated with ABC solution (1 h at room temperature) followed by 3,3′-diaminobenzidine (DAB). Later, sections were rinsed with water and counterstained with 0.25% Eosin Y for 15 s. Sections were dehydrated through a series of ethanol and xylene washes and coverslipped using ProLong™ Diamond Antifade Mountant (Invitrogen).

Results

IPSC-derived midbrain organoids display mature neuromelanin-containing dopaminergic neurons

MOs were generated from iPSCs of two PD patients carrying the L444P *GBA1* variant (either monoallelic or biallelic, denominated

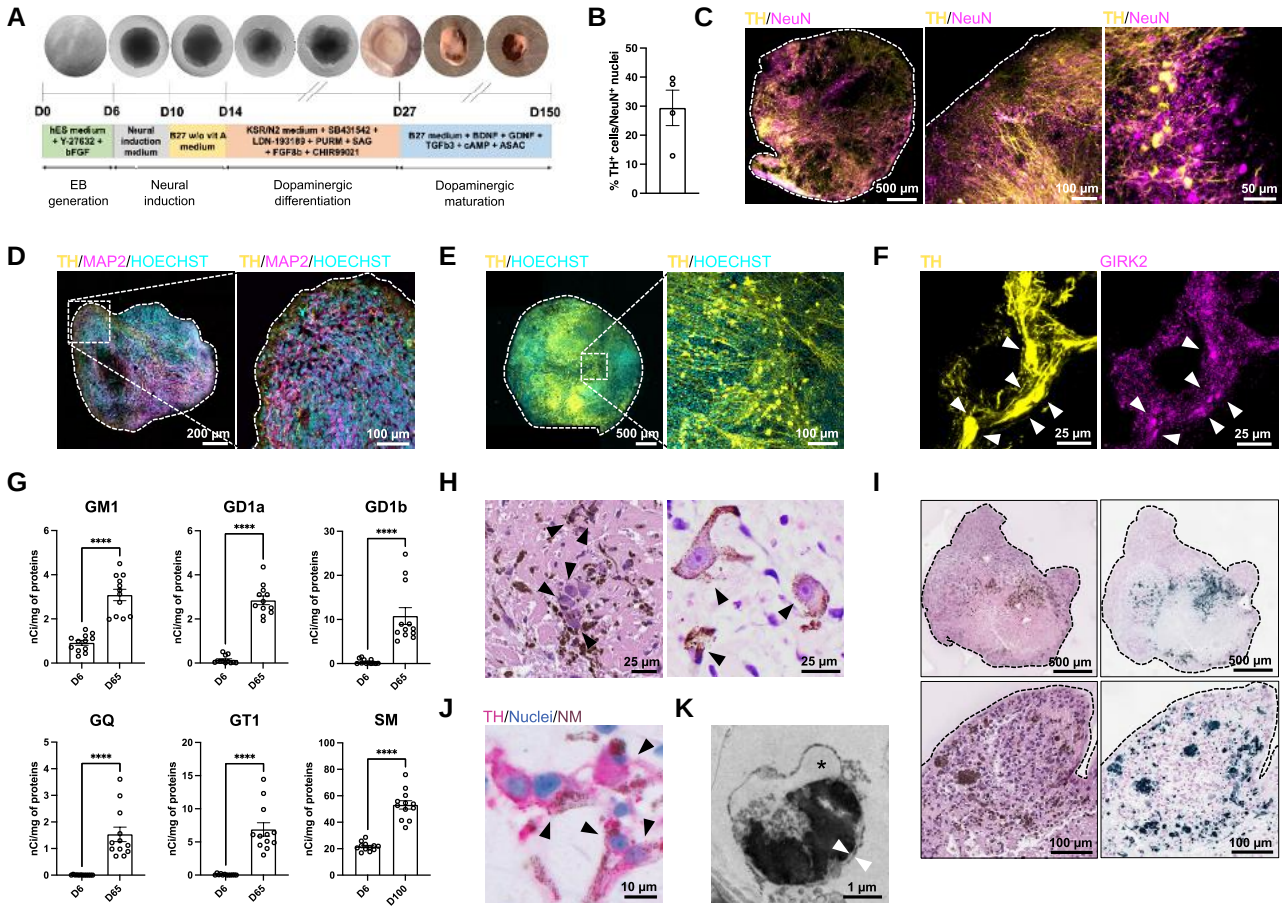

Figure 1 Midbrain organoids display mature neuromelanin-containing dopaminergic neurons. (**A**) Schematic overview of the differentiation protocol for the generation of midbrain organoids (MOs). On Day 0 (D0), induced pluripotent stem cells are seeded into ultra-low-attachment plates to allow embryoid body formation (D0–D6). Following neural induction, embryoid bodies are embedded in Cultrex (D10) and cultured in static conditions for another 4 days. On D14, tissues are transferred to spinning bioreactors, where they are subdued to dopaminergic (DA) patterning factors. Trophic factors are added on D27 to aid DA maturation and long-term culturing. (**B**) Differentiation protocol efficiency measured as quantification of TH^+ cells over $NeuN^+$ nuclei in control ($CTR1^{wt}$) midbrain organoids (MOs) at 65 days *in vitro* (DIV). $n = 4$ organoids per condition were analysed by examining whole organoid volume. (**C**) Representative immunofluorescence images of $CTR1^{wt}$ MOs at 100 DIV showing TH and NeuN expression at different magnifications. Scale bars = 50 µm (*right*), 100 µm (*middle*) and 500 µm (*left*). (**D**–**F**) Representative immunofluorescence images of neuronal and DA markers (MAP2, TH and GIRK2) expression in $CTR1^{wt}$ MOs at 65 DIV. Arrowheads in **F** indicate cell bodies of $TH^+/GIRK2^+$ DA neurons. In **D** and **E**, boxed areas are expanded in the corresponding *insets*. Scale bars = 25 µm (**F**), 100 µm (**D** *right*, **E** *right*), 200 µm (**D** *left*) and 500 µm (**E** *left*). (**G**) Sphingolipid composition of MOs (pool of CTR^{wt}, PD^{L444P} and GD/PD^{L444P} MOs) at early (6 DIV) and mature (65 or 100 DIV) time points. Fully differentiated MOs have a higher content of gangliosides and sphingomyelin enriched in human adult brain. $n = 12$ organoids for each time point; $^{****}P < 0.0001$, Student's two-tailed unpaired *t*-test. (**H**) High magnification images of haematoxylin and eosin (H&E)-stained sections of $CTR1^{wt}$ MOs at 100 DIV demonstrates neuromelanin (NM) in neurons at single-cell resolution (arrowheads). Scale bars = 25 µm. (**I**) H&E staining (*left*) and Schmorl's ferricyanide reduction method (*right*) in serial sections of $CTR2^{wt}$ (*top*) and PD^{L444P} (*bottom*) MOs at 120 DIV highlight the presence of NM pigmentation. Scale bars = 100 µm (*bottom*) and 500 µm (*top*). (**J**) Naturally pigmented NM granules (arrowheads) in TH^+ neurons (red) in $CTR2^{wt}$ MOs at 120 DIV. Scale bar = 10 µm. (**K**) Transmission electron microscopy image of GD/PD^{L444P} MO at 80 DIV showing a membrane-bound (arrowheads) pigmented organelle containing NM granules (dark-coloured pigment) and vacuolar lipid body (asterisk). Scale bar = 1 µm. In **B** and **G**, data are mean ± standard error of the mean. ASAC = ascorbic acid; bFGF = basic fibroblast growth factor; cAMP = cyclic AMP; EB = embryoid body; GIRK2 = G-protein-regulated inward-rectifier potassium channel 2; hES = human embryonic stem cell; KSR = KnockOut serum replacement; NeuN = neuronal nuclei; PURM = purmorphamine; SAG = smoothened agonist; SM = sphingomyelin; TH = tyrosine hydroxylase.

PD^{L444P} and GD/PD^{L444P}, respectively) and of three healthy control donors with wild-type *GBA1* ($CTR1^{wt}$, $CTR2^{wt}$ and $CTR3^{wt}$) (Supplementary Fig. 1 and Supplementary Table 1). Three independent clones of each line were differentiated into MOs with a novel protocol combining neuroectoderm induction[15] and ventral midbrain DA patterning[16] (Fig. 1A). IPSCs were aggregated into embryoid bodies and cultured in low-dose bFGF/high-dose ROCK inhibitor for 6 days. Embryoid bodies that developed radial neuroepithelium were embedded into hydrogel droplets and transferred to spinning bioreactors for DA patterning and long-term maturation. MOs were cultured for ≤150 DIV and collected at various time points of differentiation for extensive characterization and analyses.

Bulk RNA-sequencing (RNA-seq) profiling of differentiating MOs demonstrated progressive enrichment in neuronal and glial transcripts and in key DA markers expressed during midbrain development (Supplementary Fig. 2A). Gene ontology enrichment analyses of differentially expressed genes across maturation revealed upregulation of neuronal clusters and downregulation of cell proliferation markers (Supplementary Fig. 2B). The estimated fraction of

neurons and astrocytes within MOs based on the expression of cell-specific marker genes[19] increased at later time points of analysis (Supplementary Fig. 2C). In differentiating MOs, the level of expression of well-established neuron-specific and astrocyte-specific genes[20] increased progressively at later *in vitro* stages (Supplementary Fig. 2D and E). Specifically, expression levels of key DA genes of interest [i.e. tyrosine hydroxylase (*TH*), dopamine receptor D2 (*DRD2*) and G-protein-regulated inward-rectifier potassium channel 2 (*GIRK2*)] and of the astrocytic gene glial fibrillary protein (*GFAP*) increased linearly over time (Supplementary Fig. 2F). Fluorescent *in situ* hybridization with RNAscope revealed signals for *DRD2* and *TH* mRNA co-expression (Supplementary Fig. 2G). Genes associated with neurons of the SN and the ventral tegmental area[21] were found to be expressed in mature MOs (Supplementary Fig. 2H), indicating that DA populations of diverse midbrain areas co-exist within mature MOs.

At fully differentiated time points, ~30% of $NeuN^+$ neurons stained positive for TH (Fig. 1B and C). Within MOs, we detected widespread and extended axonal projections expressing TH, which also co-localized with the postmitotic neuronal marker MAP2 (Fig. 1D and E and Supplementary Video 1). TH^+ neurons expressed FOXA2 (Supplementary Fig. 3A), indicating floor-plate derivation, in addition to the terminal-resident proteins DAT and VMAT2 (Supplementary Fig. 3B and C), indicating synaptic maturation, and exhibited immunoreactivity for GIRK2 (Fig. 1F), which is peculiar to DA neurons. Non-DA neurons were detected by immunolabelling for the GABAergic markers GAD65 and GAD67 (Supplementary Fig. 3D and E).

Along with neuronal cells, glial elements were progressively specified in MOs during differentiation. Astrocytes were detected by positive staining for GFAP and S100B and were abundantly represented, particularly at later time points (Supplementary Fig. 3F–J). Sparse oligodendroglial elements showed immunoreactivity for OLIG2 and the myelin-associated proteins MBP and CNPase (Supplementary Fig. 3H–J), demonstrating that MOs are a composite multicellular system with the potential to reproduce neuron–glia interaction.

To investigate whether MOs recapitulate the typical membrane lipid composition of developmentally mature neurons, gangliosides were metabolically labelled at the steady state with the radioactive precursor [1-^{3}H]sphingosine. The glycosphingolipid (GSL) pattern was evaluated by high-performance thin-layer chromatography, and radioactive lipids were visualized by digital autoradiography. Over the course of differentiation, the expression pattern of GSLs changed significantly, resembling the profile transition observed during neuronal development *in vivo*.[22] Specifically, early-stage MOs presented with a high content of GM3 and lower amounts of GM2, GM1 and GD1a components, whereas fully differentiated MOs at 65 DIV were enriched in all polysialogangliosides found in mature neurons of the adult brain, in addition to sphingomyelin, signifying their mature identity (Fig. 1G and Supplementary Fig. 3K and L).

As early as 35 DIV, we observed the appearance of pigmentation in the form of granular spots on the surface of MOs (Fig. 1A and Supplementary Fig. 4A). High-magnification brightfield microscopy imaging of haematoxylin- and eosin-stained sections showed that the pigment was contained in cells with neuronal morphology (Fig. 1H and I and Supplementary Fig. 4B and C). Schmorl's ferricyanide reduction method for melanic pigments detected sites of reduction activity in MOs, which appeared as large, blue-stained granules within the neuronal cytosol, similar to deposits observed in human post-mortem SN sections (Fig. 1I and Supplementary Fig. 4D). Melanin sites corresponded to the same pigmented areas already visible in haematoxylin- and eosin-stained slides, suggesting that the brown pigment contained within MOs was a type of melanin (Fig. 1I). To discriminate the pigment, we performed a red chromogen labelling of TH and identified pigmented granules in the cytoplasm of TH^+ cells, which indicated the content of a type of melanin within DA neurons (Fig. 1J and Supplementary Fig. 4E). To characterize the biosynthetic process of the pigment, we performed staining for tyrosinase (TYR), which catalyses the production of cutaneous melanin, but not of neuromelanin.[23] First, we validated the antibody in a section of a nevus, which showed immunoreactivity for TYR and lack of expression of TH (Supplementary Fig. 4F). Pigmented neurons in MOs and in the SN section of a healthy donor subject displayed immunostaining of TH, but not of TYR (Supplementary Fig. 4F), suggesting that the melanin contained in MOs was, in fact, neuromelanin. Electron-dense, membrane-bound granules 2–3 µm in size, some presenting a vacuolar lipid body, were detected in pigmented cells (Fig. 1K and Supplementary Fig. 4G), thereby recapitulating the ultrastructural features of naturally occurring neuromelanin in human SN.[24] Neuromelanin content increased progressively over time, covering up to ~80% of the total surface area of MOs at later stages of differentiation (Supplementary Fig. 4H).

Finally, the observation of Ca^{2+} transients in MOs indicated cellular activity, which was recorded in both basal conditions and upon incubation with either glutamic acid or dopamine (Supplementary Fig. 5A–G and Supplementary Videos 2 and 3). To image Ca^{2+} events at a single-cell resolution, MOs were enzymatically dissociated into bidimensional cultures. Individual cells with typical neuronal morphology exhibited spontaneous Ca^{2+} surges of longer duration and lower firing rate, suggesting that a 3D organization might contribute to activity complexity (Supplementary Video 4). Administration of tetrodotoxin suppressed Ca^{2+} events, indicating their dependence on Na^+ channel functional integrity (Supplementary Video 5).

Collectively, these results demonstrate that MOs contain mature DA neurons with postnatal nigral identity, resembling those found in human adult SN.

ER-retained mutant GCase leads to GlcCer increase in *GBA1*-PD midbrain organoids

GCase activity is reduced in brains and CSF of PD patients with and without mutations in *GBA1* and is associated with increased levels of α-syn in brains of PD subjects.[25,26] However, whether GCase deficiency in PD leads to substrate accumulation and how GlcCer is implicated in the pathogenesis is still controversial.[27–30]

To establish a pharmacological model of GCase deficiency, CTR^{wt} MOs were treated with the GCase irreversible inhibitor conduritol B epoxide (CBE), which resulted in complete suppression of GCase activity (Fig. 2A). GD/PD^{L444P} MOs presented a marked reduction in the residual enzymatic activity (Fig. 2B). In PD^{L444P} MOs and in the SN of the PD^{L444P} donor patient (SNc_PD^{L444P}), GCase activity was reduced by ~50% with respect to wild-type *GBA1* MOs (Fig. 2B and C). Likewise, the reduction in the amount of GCase protein observed in SNc_PD^{L444P} was reproduced in PD^{L444P} MOs (Fig. 2D–F and Supplementary Fig. 6A). GCase protein content was also reduced in GD/PD^{L444P} MOs and in CBE-treated CTR^{wt} MOs (Fig. 2D and E and Supplementary Fig. 6B and C).

To follow the intracellular fate of GCase, we treated cell lysates with endoglycosidase H (endo-H), which can discriminate glycoproteins retained in the ER from those that have reached the mid-Golgi. In PD^{L444P} and GD/PD^{L444P} MOs (Supplementary Fig. 6D)

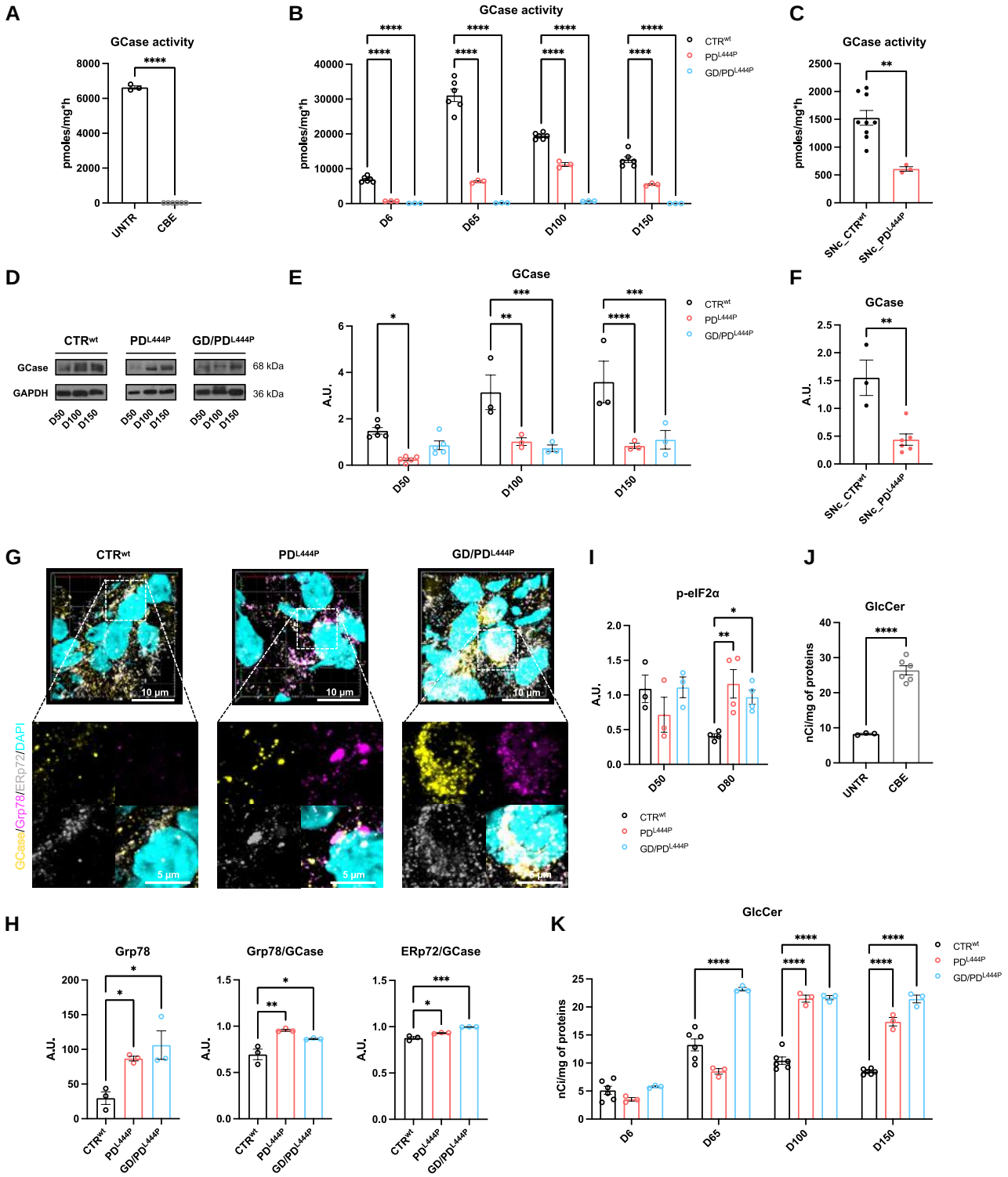

Figure 2 *GBA1* L444P mutation results in reduced enzyme activity, endoplasmic reticulum retention of mutant glucocerebrosidase and increased levels of glucosylceramide. (**A**) Glucocerebrosidase (GCase) enzymatic activity in control (CTR^{wt}) midbrain organoids (MOs) at 65 days *in vitro* (DIV) with and without treatment with 500 µM conduritol B epoxide (CBE) for 14 days. $n = 9$ organoids; $^{****}P < 0.0001$, Student's two-tailed unpaired *t*-test. (**B**) GCase enzymatic activity in CTR^{wt}, Parkinson's disease heterozygous L444P *GBA1* mutation (PD^{L444P}) and Gaucher's disease (GD)/PD^{L444P} MOs at 6, 65, 100 and 150 DIV. $n = 3$ biological replicates per line for each time point; $^{****}P < 0.0001$, two-way ANOVA with Dunnett's *post hoc* test. (**C**) GCase enzymatic activity in substantia nigra pars compacta (SNc)_CTR^{wt} and SNc_PD^{L444P} brain extracts. $n = 12$ samples; $^{**}P < 0.01$, Student's two-tailed unpaired *t*-test. (**D** and **E**) Representative western blots and relative densitometries showing GCase levels in CTR^{wt}, PD^{L444P} and GD/PD^{L444P} MOs at 50, 100 and 150 DIV. $n = 33$ organoids; $^{****}P < 0.0001$, $^{***}P < 0.001$, $^{**}P < 0.01$, $^{*}P < 0.05$, two-way ANOVA with Dunnett's *post hoc* test. (**F**) Densitometry of GCase/GAPDH amount in brain extracts from patients. $n = 9$ samples; $^{**}P < 0.01$, Student's two-tailed unpaired *t*-test. (**G**) Representative images of CTR^{wt}, PD^{L444P} and GD/PD^{L444P} MOs at 100 DIV immunolabelled for GCase, Grp78 and ERp72. Indicated regions are expanded in the *insets* (*bottom*). Scale bars = 5 µm (*bottom*) and 10 µm (*top*). (**H**) Quantification of Grp78, Grp78/GCase co-localization and ERp72/GCase co-localization from

(Continued)

and fibroblasts (not shown), most of GCase was endo-H sensitive, in line with previous observations in mutant *GBA1* models.[11,31,32] By immunofluorescence analysis, we found that the ER protein Grp78, which can activate the unfolded protein response (UPR) upon interaction with misfolded proteins accumulated in the ER, was increased in PD^{L444P} and GD/PD^{L444P} MOs (Fig. 2G and H and Supplementary Fig. 6E). Given that the levels of Grp78 are increased upon prolonged UPR activation, this would support the occurrence of ER stress.[33] Extensive co-localization of GCase with both Grp78 and the ER resident protein ERp72 in *GBA1* mutant MOs corroborated that most of the GCase protein was retained in the ER, likely in misfolded conformation (Fig. 2G and H and Supplementary Fig. 6E). Moreover, we detected increased levels of phospho-eIF2α in both PD^{L444P} and GD/PD^{L444P} MOs at 80 DIV, supporting activation of the UPR, probably induced by ER-retained GCase (Fig. 2I and Supplementary Fig. 6F). Interestingly, by western blot analysis we found that the levels of Grp78 were higher in total protein extracts of PD^{L444P}, but not of GD/PD^{L444P} (Supplementary Fig. 6F and G), which might either indicate the occurrence of augmented ER stress in *GBA1*-related PD only or might reflect a higher cell loss in GD/PD^{L444P} MOs. Transmission electron microscopy analysis showed a dilated morphology of the ER lumen in *GBA1*-PD MOs, as seen in conditions of ER membrane expansion under ER stress[33] (Supplementary Fig. 6H). In contrast, in CTR^{wt} MOs only a fraction of GCase was located in the ER, but scarcely co-localized with Grp78 (Fig. 2G and H and Supplementary Fig. 6E).

We then explored whether the deficiency of GCase might lead to substrate accumulation. By metabolically labelling glycosphingolipids with [1-^{3}H]sphingosine, we observed accumulation of GlcCer in CBE-treated CTR^{wt} (Fig. 2J and Supplementary Fig. 6I). Of particular interest, *GBA1* mutant MOs also showed elevated levels of GlcCer, already observed at 65 DIV in GD/PD^{L444P} MOs and at 100 DIV in PD^{L444P} MOs (Fig. 2K and Supplementary Fig. 6J).

GBA1-PD midbrain organoids reproduce dopaminergic neurodegeneration and Lewy-like pathology

The degeneration of DA nigrostriatal neurons and the accumulation of insoluble α-syn in LBs and LNs are the defining neuropathological hallmarks of PD. *GBA1*-related PD brains also display neurodegeneration and Lewy pathology, as much as brains of GD patients with PD.[34,35]

We aimed to evaluate the capability of *GBA1* MOs to recapitulate DA neuron loss and to reproduce a clear α-syn pathology, as seen in PD brains, and its relationship to mutant GCase. For this purpose, we initially quantified the number of TH$^+$ cells versus the total number of NeuN$^+$ neurons in TDE-clarified whole MOs by 3D confocal microscopy analysis and found a reduction in the amount of DA neurons in *GBA1* mutant MOs at 100 DIV, which was slightly more significant in GD/PD^{L444P} (Fig. 3A and B).

The analysis of total α-syn showed an incremental accumulation of the protein over time in TH$^+$ DA neurons of *GBA1*-PD MOs starting from 50 DIV (Fig. 3C and Supplementary Fig. 7A) and a higher content in PD^{L444P} and SNc_PD^{L444P} and after CBE treatment (Supplementary Fig. 7B–G). Notably, α-syn was detected in urea/sodium dodecyl sulfate (SDS) reconstituted detergent-insoluble protein fraction from GD/PD^{L444P} and PD^{L444P} MOs as early as 60 and 80 DIV, respectively (Fig. 3D and E). Likewise, CBE-treated CTR^{wt} MOs also exhibited detergent-insoluble α-syn (Supplementary Fig. 7H and I).

To explore the aggregation state of detected insoluble α-syn further, we performed both fluorescent and chromogenic immunohistochemistry by initially treating slides with PK, then staining with two antibodies developed against fibrillary components of LBs. Remarkably, as of 80 DIV, *GBA1* mutant MOs and CBE-treated samples displayed abundant insoluble Lewy-like deposits, resembling the neuropathology of the brain of the donor patient (Fig. 3F and G and Supplementary Fig. 7J–L). Lewy-like aggregates displayed heterogeneous morphologies, ranging from diffuse cytoplasmic staining to discrete, packed structures and doughnut-shaped inclusions, reminiscent of mature LBs (Fig. 3H). Notably, both PD^{L444P} and GD/PD^{L444P} MOs also presented aggregated α-syn-immunoreactive neuronal processes, which were suggestive of Lewy-like neurites (Fig. 3I). In *GBA1*-mutated MOs, TH$^+$ neurons also exhibited marked immunopositivity for α-syn phosphorylated at serine 129 (S129), a predominant post-translationally modified form of α-syn within LBs (Fig. 3J and K).[36,37] Additionally, double chromogenic immunostaining showed that α-syn inclusions in *GBA1*-PD MOs were also ubiquitinated (Supplementary Fig. 7M), like LBs in PD brains.[38]

To provide an ultrastructural characterization of aggregates and a validation of LB-like pathology, we performed transmission electron microscopy imaging, which revealed perinuclear inclusions of electron-dense material and membrane fragments within large autophagic vacuolar-like structures in *GBA1* MOs (Fig. 3L and Supplementary Fig. 8A). In some cells, the entire cytoplasm appeared to be crowded with membranous material originating from fragmented organelles (e.g. mitochondria, lysosomes and autophagosomes), tubulovesicular structures, distorted vacuoles, lipids, randomly distributed filaments and disrupted cytoskeleton (Fig. 3M and Supplementary Fig. 8B–D). Such features were fully reminiscent of the composition of bona fide LBs as detected by correlative light and electron microscopy and tomography in post-mortem PD brains.[5]

Taken together, these findings demonstrate that MOs from *GBA1* patients recapitulate fundamental morphological, immunohistochemical and ultrastructural features of Lewy pathology.

α-Synuclein produced in GBA1 midbrain organoids seeds Parkinson's disease pathology

Evidence from PD brains and mouse models suggests that α-syn fibrils template the aggregation of endogenous α-syn and spread the pathology in interconnected neurons.[39] In our study, amyloid fibrils were found by transmission electron microscopy analysis of the insoluble α-syn fraction extracted from PD^{L444P} and GD/PD^{L444P} MOs (Supplementary Fig. 8E). Thioflavin-S (Thio-S) staining further demonstrated aggregates of fibrillary α-syn within TH$^+$ neurons in *GBA1* mutant and CBE-treated MOs (Fig. 4A–D and Supplementary Fig. 8F). To explore the seeding properties of the pathological

Figure 2 Continued
immunofluorescent images shown in **G**. $n = 3$ biological replicates per line; $^{***}P < 0.001$, $^{**}P < 0.01$, $^{*}P < 0.05$, one-way ANOVA with Tukey's *post hoc* test. (**I**) Densitometry of p-eIF2α/GAPDH amount in CTR^{wt}, PD^{L444P} and GD/PD^{L444P} MOs at 50 and 80 DIV. $n = 21$ organoids; $^{**}P < 0.01$, $^{*}P < 0.05$, two-way ANOVA with Dunnett's *post hoc* test. (**J** and **K**) Glucosylceramide (GlcCer) levels in CTR^{wt} MOs at 65 DIV following treatment with CBE (**J**) and in CTR^{wt}, PD^{L444P} and GD/PD^{L444P} MOs at 6, 65, 100 and 150 DIV (**K**) evaluated by the metabolic labelling at the steady state using radioactive sphingosine. In **J**: $n = 9$ organoids; $^{****}P < 0.0001$, Student's two-tailed unpaired *t*-test; in **K**: $n = 3$ biological replicates per line for each time point; $^{****}P < 0.0001$, two-way ANOVA with Dunnett's *post hoc* test. In **A–C**, **E**, **F** and **H–K**, data are mean ± standard error of the mean. A.U. = arbitrary units; UNTR = untreated.

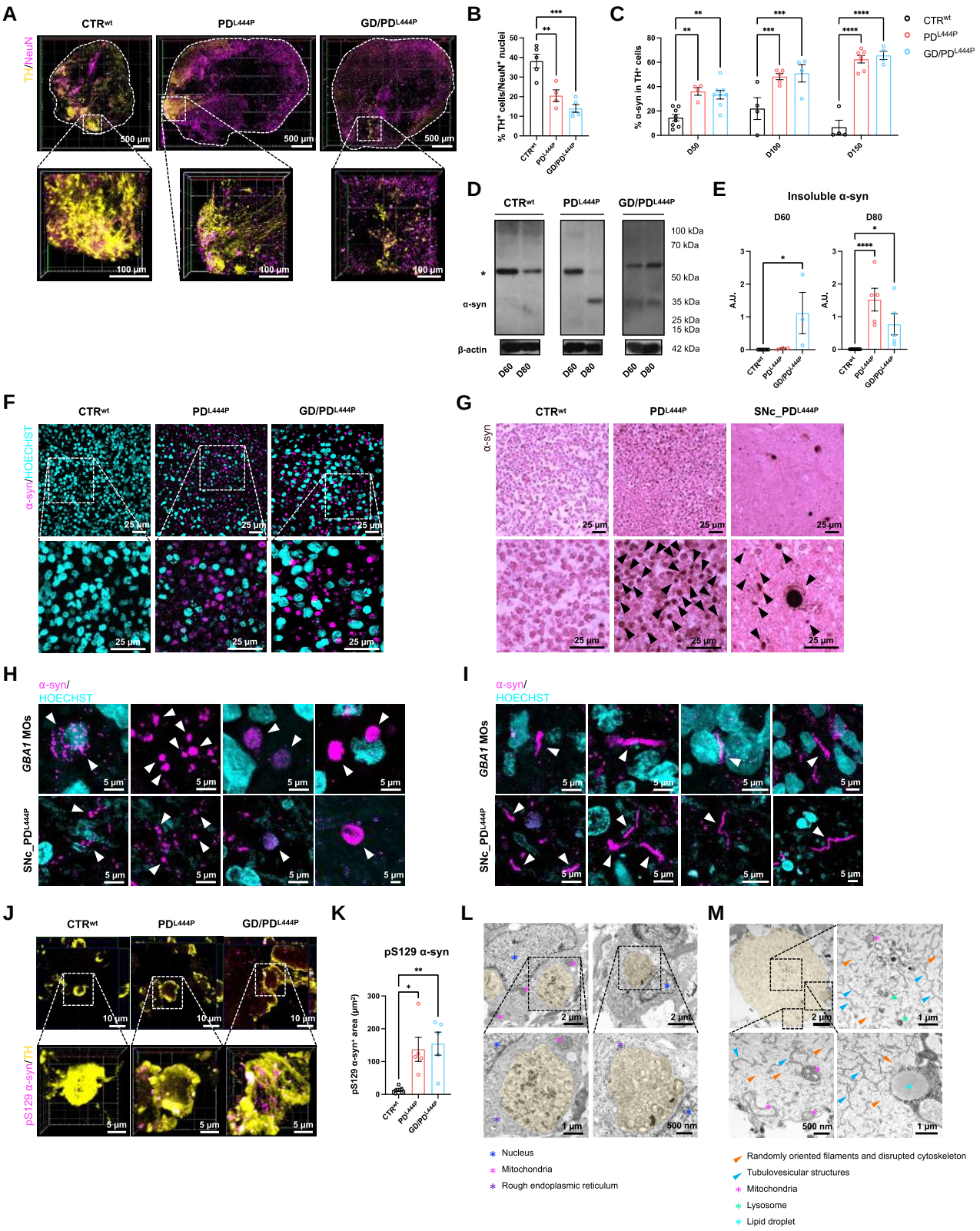

Figure 3 *GBA1*-Parkinson's disease midbrain organoids reproduce dopaminergic neurodegeneration and Lewy-like pathology. (**A** and **B**) Immunofluorescence labelling of TDE-clarified control (CTR^{wt}), Parkinson's disease heterozygous L444P *GBA1* mutation (PD^{L444P}) and Gaucher's disease (GD)/PD^{L444P} midbrain organoids (MOs) at 100 days *in vitro* (DIV) and relative 3D confocal microscopy analysis of TH^+ and $NeuN^+$ cells showing dopaminergic (DA) neuron loss in *GBA1* mutant MOs. **A** shows orthogonal *z*-stack projections. $n = 14$ organoids, with each value in **B** corresponding to analysis conducted on individual whole organoids; $^{***}P < 0.001$, $^{**}P < 0.01$, one-way ANOVA with Dunnett's *post hoc* test. Scale bars = 100 µm (*bottom*) and 500 µm (*top*). (**C**) Analysis of the progressive accumulation of α-synuclein (α-syn) in TH^+ neurons in *GBA1* mutant MOs from immunostaining shown in Supplementary Fig. 7A. $n = 2$ organoids of each line were analysed by examining an average of five fields per condition; $^{****}P < 0.0001$,

(Continued)

form of α-syn found in the insoluble fraction, we performed a seed amplification assay for ultrasensitive detection of aggregated α-syn. PD^{L444P} and GD/PD^{L444P} MOs induced an efficient seeding activity for recombinant α-syn, as seen with SNc_PD^{L444P} and brain homogenates of subjects with α-synucleinopathy (Fig. 4E and Supplementary Fig. 8G).

To corroborate the ability of α-syn fibrils from *GBA1*-PD MOs to self-propagate and induce aggregation in healthy cells, we injected PD^{L444P} MO-extracted α-syn insoluble fractions into CTR^{wt} MOs. Two weeks after the inoculation of fibrils from donor PD^{L444P} MOs, injected CTR^{wt} MOs developed Thio-S^{+}/α-syn^{+} aggregates similar to those previously observed in the donor PD^{L444P} MOs (Fig. 4F and G).

These data indicate that α-syn produced in PD MOs shares similar seeding properties to that observed in PD brains.

α-Synuclein–synapsin III interplay in *GBA1*-PD midbrain organoids

We then explored whether *GBA1* MOs might exhibit changes in the levels of synapsin III (Syn III), a presynaptic phosphoprotein co-accumulating and co-localizing with α-syn in LBs as it sticks to α-syn fibrils[14] and which acts as a key mediator of α-syn aggregation and toxicity.[40,41] In *GBA1*-PD MOs and in SNc_PD^{L444P}, we observed a significantly higher amount of Syn III, consistent with previous observations in PD brains (Supplementary Fig. 9A–D). Interestingly, Syn III levels increased earlier in biallelic *GBA1* MOs and later in the monoallelic *GBA1* mutants. Syn III also exhibited an increase, albeit not significant, after inhibition of GCase activity with CBE (Supplementary Fig. 9E and F). When we investigated the distribution of the protein in TH^{+} neurons, we found that PD^{L444P} and GD/PD^{L444P} MOs exhibited a marked co-accumulation of Syn III and α-syn, which were found to co-localize abundantly (Supplementary Fig. 9G and H), as observed in post-mortem PD brains.[14] Notably, levels of Syn III and α-syn showed a positive linear correlation in PD^{L444P} and GD/PD^{L444P} MOs (Supplementary Fig. 9I), corroborating the synergistic pathological interplay of these proteins in PD.[14]

Glucocerebrosidase pathway modulation rescues α-synuclein pathology

Finally, we tested the capability of two compounds engaging with the GCase pathway ultimately to counteract neuronal loss and α-syn pathological deposition in *GBA1*-mutated MOs.

First, we treated MOs with ambroxol, a small molecule chaperone with proven efficacy in overcoming the retention of mutant GCase in the ER and in improving GCase activity.[32,42] Ambroxol administration led to an increase in the amount of GCase protein in MOs of all lines (Fig. 5A and B) and restored GCase enzymatic activity to normal levels in PD^{L444P} MOs, whereas it did not affect GCase activity in GD/PD^{L444P} MOs (Supplementary Fig. 10A). In PD^{L444P} and GD/PD^{L444P} MOs, the amount of GlcCer was not influenced by ambroxol treatment (Fig. 5E and Supplementary Fig. 10B). The higher co-localization between GCase and the lysosomal marker LAMP1 supported that ambroxol increased GCase targeting to the lysosome in both PD^{L444P} and GD/PD^{L444P} MOs (Fig. 5G and Supplementary Fig. 10C). In PD^{L444P} MOs, this was also accompanied by a reduction of the Grp78/GCase co-localization, suggesting a reduction of the misfolded fraction (Supplementary Fig. 10D–F). We then explored whether the observed effects of ambroxol on GCase activity and protein levels had an impact on DA neuron viability and α-syn pathology. Treatment with ambroxol rescued DA loss in PD^{L444P} MOs and improved, although not significantly, neuronal survival in GD/PD^{L444P} (Supplementary Fig. 11A and B). Ambroxol reduced the amount of total α-syn and Syn III in all samples (Supplementary Fig. 11C–F). Notably, the number and the area of PK-resistant α-syn aggregates were strongly reduced in *GBA1*-PD MOs (Fig. 5H and I and Supplementary Fig. 11G).

Second, we tested the effect of GZ667161, an experimental GlcCer synthase inhibitor that has been shown to decrease the levels of GlcCer and α-syn aggregates in *GBA1*$^{D409V+/+}$ and *SNCA*^{A53T} rodent models.[43] Upon treatment, GlcCer levels were undetectable (Fig. 5F and Supplementary Fig. 11H) and the amount of GCase protein was reduced in all samples (Fig. 5C and D). GZ667161 improved the relocation of GCase to the lysosomal compartment, although this was significant only in GD/PD^{L444P} (Fig. 5G and Supplementary Fig. 10C), in which lysosomal accumulation of GlcCer is the main biochemical consequence of the enzymatic deficiency. These data might indicate that acting on lysosomal engorgement by reducing substrate accumulation could improve the upstream targeting of GCase from the ER to the lysosome. Importantly, GZ667161 reduced Grp78/GCase co-localization in PD^{L444P} MOs, suggesting also an effect on misfolding of GCase (Supplementary Fig. 10D–F). Cell counts of TH^{+} cells showed that GZ667161 did not preserve DA neurons in PD^{L444P} and GD/PD^{L444P} (Supplementary Fig. 11A and B). Interestingly, levels of total α-syn were unaffected in *GBA1* MOs, although they were reduced in CTR^{wt} MOs (Supplementary Fig. 11I and J). However, GZ667161 treatment markedly reduced the load

Figure 3 Continued
***P < 0.001, **P < 0.01, two-way ANOVA with Tukey's *post hoc* test. (**D** and **E**) Representative western blots and relative densitometry of detergent-resistant insoluble α-syn fractions in CTR^{wt}, PD^{L444P} and GD/PD^{L444P} MOs at 60 and 80 DIV. Asterisk indicates a non-specific 55 kDa band. $n = 3$ biological replicates per line at 60 DIV, $n = 5$ biological replicates per line at 80 DIV; ****P < 0.0001, *P < 0.05, one-way ANOVA with Dunnett's *post hoc* test. (**F**) Representative immunofluorescence images of proteinase K (PK)-resistant insoluble α-syn immunoreactivity in CTR^{wt}, PD^{L444P} and GD/PD^{L444P} MOs at 80 DIV. Scale bars = 25 µm. (**G**) DAB (3,3′-diaminobenzidine) immunoreactivity of α-syn in Eosin Y-stained CTR^{wt}, PD^{L444P} and GD/PD^{L444P} MOs at 80 DIV and in substantia nigra pars compacta (SNc)_PD^{L444P} following treatment with PK. Arrowheads indicate PK-resistant inclusions of insoluble α-syn. Scale bars = 25 µm. (**H** and **I**) High-magnification images of PK-resistant α-syn organization in MOs from subjects carrying L444P *GBA1* mutations at 100 DIV and in SNc_PD^{L444P}: heterogeneous morphology of α-syn inclusions might be indicative of various stages of maturation of Lewy body-like aggregates (**H**) and Lewy neurite-like processes (**I**) reminiscent of Lewy pathology seen in human brains (arrowheads). Scale bars = 5 µm. (**J** and **K**) Immunostaining of α-syn phosphorylated at serine 129 (pS129 α-syn) inclusions in TH^{+} neurons (**J**) and quantification of pS129 α-syn^{+} area (**K**) in CTR^{wt}, PD^{L444P} and GD/PD^{L444P} MOs at 100 DIV. **J** shows orthogonal z-stack projections. $n = 5$ biological replicates per line, with each point representing the mean of three z-stack images for each organoid; **P < 0.01, *P < 0.05, one-way ANOVA with Dunnett's *post hoc* test. Scale bars, 5 µm (*bottom*) and 10 µm (*top*). (**L**) Representative transmission electron microscopy (TEM) images of PD^{L444P} (*left*) and GD/PD^{L444P} (*right*) MOs at 80 DIV showing large autophagosome/autolysosome-like bodies with inclusions of aggregated intracellular material in the perinuclear region. Cellular organelles are indicated by asterisks and in the corresponding legend. Scale bars = 500 nm (*bottom right*), 1 µm (*bottom left*) and 2 µm (*top*). (**M**) Representative TEM images of a Lewy-like inclusion in PD^{L444P} MO at 80 DIV. Disrupted cytoskeleton and filaments (orange arrowheads), tubulovesicular structures (blue arrowheads), lipid droplet (aqua asterisk), abundant membrane fragments from mitochondria (pink asterisks) and lysosomes (green asterisks) are visible. Scale bars = 500 nm (*bottom left*), 1 µm (*right*) and 2 µm (*top left*). In **B**, **C**, **E** and **K**, data are mean ± standard error of the mean. Boxed areas are expanded in the corresponding *insets*. A.U. = arbitrary units; TDE = 2,2′-thiodiethanol; TH = tyrosine hydroxylase.

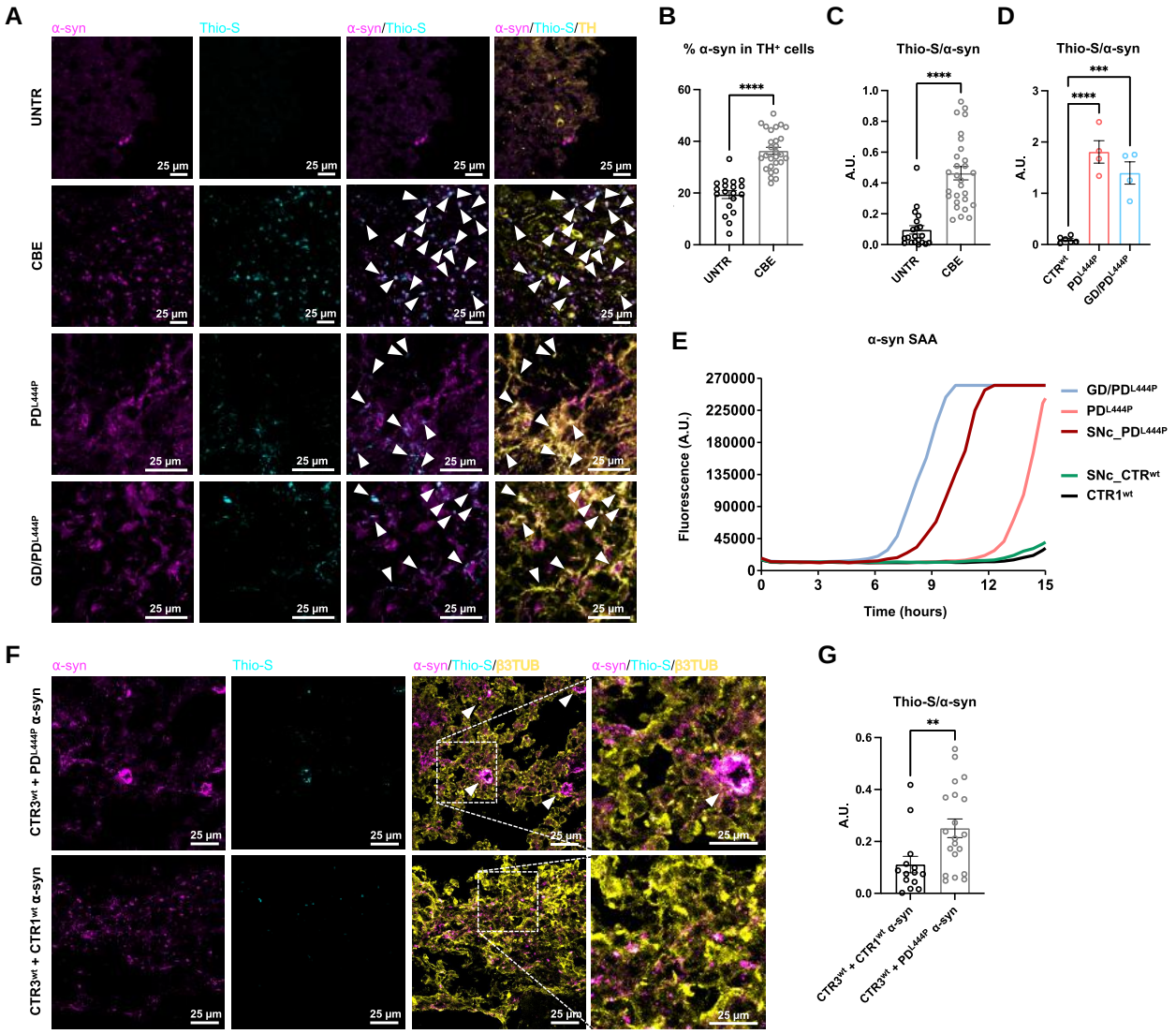

Figure 4 Insoluble α-synuclein from *GBA1* midbrain organoids induces aggregation of endogenous α-synuclein. (**A**) Representative immunofluorescence images of α-synuclein (α-syn)$^+$/thioflavin-S (Thio-S)$^+$ aggregates in TH$^+$ neurons in Parkinson's disease heterozygous L444P *GBA1* mutation (PD^{L444P}) and Gaucher's disease (GD)/PD^{L444P} midbrain organoids (MOs) at 100 days *in vitro* (DIV) and in conduritol B epoxide (CBE)-treated control (CTR^{wt}) MOs. Arrowheads indicate inclusions of fibrillary α-syn with double staining for α-syn and Thio-S. Scale bars = 25 µm. (**B**) Analysis of the percentage of α-syn in TH$^+$ neurons in CTR^{wt} MOs at 100 DIV following CBE treatment shown in **A**. $n = 3$ organoids per condition; $^{****}P < 0.0001$, Student's two-tailed unpaired *t*-test. (**C**) Analysis of the overlay area of Thio-S/α-syn in CBE-treated CTR^{wt} MOs at 100 DIV shown in **A**. $n = 3$ organoids per condition; $^{****}P < 0.0001$, Student's two-tailed unpaired *t*-test. (**D**) Analysis of the overlay area of Thio-S/α-syn in CTR^{wt}, PD^{L444P} and GD/PD^{L444P} MOs at 100 DIV shown in **A**. $n = 14$ organoids; $^{****}P < 0.0001$, $^{***}P < 0.001$, one-way ANOVA with Tukey's *post hoc* test. (**E**) Aggregation kinetics of recombinant α-syn induced by CTR^{wt}, PD^{L444P} and GD/PD^{L444P} MOs at 100 DIV and brain homogenates of the PD^{L444P} patient [substantia nigra pars compacta (SNc)_PD^{L444P}] and one control subject (SNc_CTR^{wt}). (**F**) Representative immunofluorescence images of α-syn and Thio-S-labelled aggregates in β-3 tubulin (β3TUB)$^+$ neurons in CTR3^{wt} MOs at 100 DIV previously injected with α-syn extracted from PD^{L444P} MOs or CTR1^{wt} MOs at 100 DIV. Arrowheads indicate inclusions of fibrillary α-syn with double staining for α-syn and Thio-S. Boxed areas are expanded in the *insets* on the *right*. Scale bars = 25 µm. (**G**) Analysis of the overlay area of Thio-S/α-syn in CTR3^{wt} MOs following injection of α-syn from data shown in **F**. $n = 4$ organoids per condition; $^{**}P < 0.01$, Student's two-tailed unpaired *t*-test. In **B–E** and **G,** data are mean ± standard error of the mean. A.U. = arbitrary units; SAA = seed amplification assay; UNTR = untreated.

of PK-resistant α-syn aggregates and lowered Syn III levels (Fig. 5H and I and Supplementary Fig. 11G, K and L).

Discussion

The elucidation of pathogenic processes underlying neurodegeneration and development of novel therapies for PD both demand an experimental system that can recapitulate distinctive features of the human brain and fundamental hallmarks of neuropathology observed in patients. The bidimensional human cell models generated so far have failed to reproduce faithfully the characteristic features of DA neurons with mature SN-like identity and to replicate cardinal neuropathological signatures of PD. The advent of 3D cultures of human DA neurons and midbrain-like organoids has reinvigorated this field.[44-49] Expanding this line of research, we devised a novel method for the generation of MOs that combines induction of neuroectoderm and DA patterning, ultimately

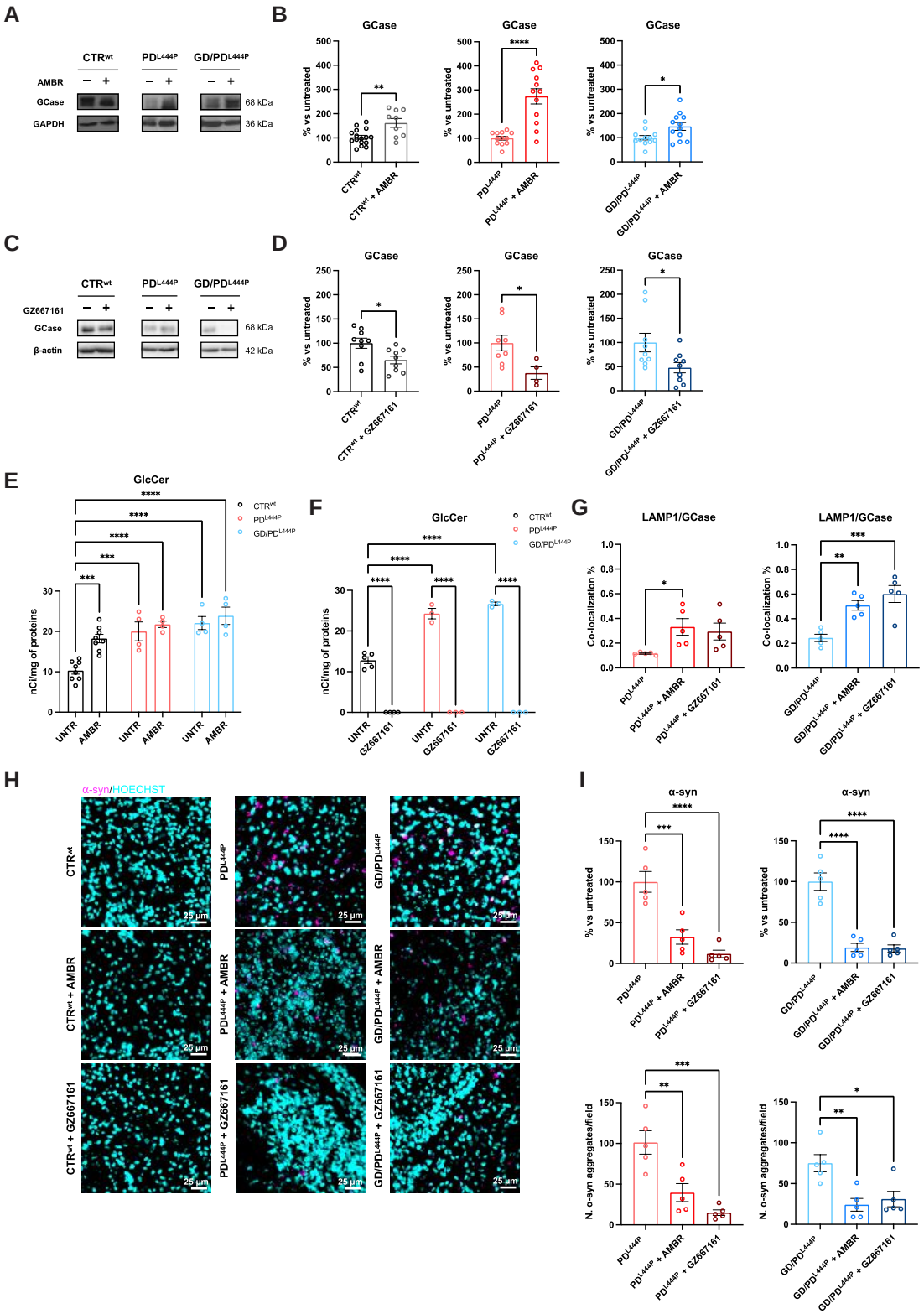

Figure 5 Rescue of glucocerebrosidase pathway and α-synuclein pathology with ambroxol and GZ667161. (**A**–**D**) Representative western blots and relative densitometry of glucocerebrosidase (GCase) levels in control (CTR^{wt}), Parkinson's disease with heterozygous L444P *GBA1* mutation (PD^{L444P}) and Gaucher's disease (GD)/PD^{L444P} midbrain organoids (MOs) at 100 days *in vitro* (DIV), with and without treatment with ambroxol (AMBR) (100 μM for 10 days; **A** and **B**) or GZ667161 (100 nM for 14 days; **C** and **D**), calculated as percentage changes with respect to untreated. $n = 4$–16 organoids per condition; $^{****}P < 0.0001$, $^{**}P < 0.01$, $^{*}P < 0.05$, Student's two-tailed unpaired *t*-test. (**E** and **F**) Glucosylceramide (GlcCer) levels of CTR^{wt}, PD^{L444P} and GD/PD^{L444P} MOs at 100 DIV with and without treatment with AMBR or GZ667161, evaluated by metabolic labelling at the steady state using [1-^{3}H]sphingosine. $n = 4$ biological replicates per line per condition in **E**; $n = 3$–5 biological replicates per line per condition in **F**; $^{****}P < 0.0001$, $^{***}P < 0.001$,

(Continued)

allowing an advanced maturation state of neurons and glial cells. Unlike previously described methods for MO generation,[44-48] which apply DA patterning at the start of differentiation, the first part of our protocol consists of unpatterned development of neuroepithelium and promotes the outgrowth and proliferation of neural progenitors, which are later subdued to small molecules guiding ventral midbrain development through activation of WNT signalling and SHH pathways. The timing of the start of the DA patterning at a later stage might favour a physiologically relevant environment in which a proportion of neural progenitors efficiently differentiate into DA neurons, while other precursors that have been committed, in part, to a non-DA fate (e.g. other neuronal types, glia cells) continue their differentiation path.

The progressively increasing expression of midbrain-specific transcripts and proteins in MOs supported their ability to reproduce key characteristics of adult human midbrain neurons, with both SN and ventral tegmental area identity. The additional presence of cells expressing GABAergic and glial-specific markers further showed MOs to be a comprehensive multi-culture system mimicking the *in vivo* conditions.

The development of neuromelanin in MOs and its striking abundance at later stages of differentiation provided further evidence of the postnatal identity of our model. In human midbrain, neuromelanin contained in DA neurons confers the characteristic pigmentation of the SN, becoming apparent after the third year of life and increasing in amount with age.[23] Although previous studies based on MO cultures claimed the presence of neuromelanin,[44,45,50-52] the lack of a full characterization of the observed pigment did not enable such evidence to be clearly substantiated. Here, we determined whether the pigment developed by our MOs had the defining characteristics of naturally occurring neuromelanin of the human midbrain, according to stringent structural and immunohistochemical criteria.[23,24,53] The characterization of such pigment contained in electron-dense membrane-bound organelles exhibiting vacuolar lipid bulbs and progressively enriched in TH^+/TYR^- neurons demonstrated that our MO model develops neuromelanin granules in DA cells.

We then aimed at exploring the capability of MOs to model key *GBA1*-PD neuropathological features. To this end, we selected two subjects affected by PD and carrying the *GBA1* L444P mutation, which is the most common genetic risk factor for PD worldwide.[7] The implications of *GBA1* pathogenic variants in the pathogenesis of PD are still a matter of debate.[13] The known impact of GCase activity impairment in GD prompted studies investigating whether and how the enzymatic deficit could favour the aggregation of α-syn in neurons of *GBA1*-PD patients.[10,54] Interestingly, GlcCer accumulation has been reported in the SN of PD brains independently of *GBA1* mutational status.[27] However, in studies conducted on extra-nigral areas (i.e. striatum, cerebellum and cortex) of brains of PD subjects, substrate accumulation was not detected.[28-30] Whether this discrepancy is related to the fact that brain regions not primarily affected in PD might be less prone to show GlcCer accumulation or that substrate is not accumulated in PD still needs to be elucidated. Moreover, it is feasible that GlcCer accumulation might not be detectable in PD brains owing to the loss of specific neuronal populations. In this regard, MOs can be evaluated before extensive neuronal loss occurs, thus allowing lipid dysregulation and toxic accumulation to be captured in the surviving DA neurons. Furthermore, by recapitulating features of the adult brain, the MO system allows a faithful reproduction of lipid metabolism occurring in neurons, thus allowing exploration of the repercussions of GlcCer metabolism on α-syn pathology. In line with the enzymatic/substrate hypothesis, *GBA1*-mutated MOs displayed a reduced GCase activity, a time-dependent increase in GlcCer levels and substantial Lewy-like pathology. To the best of our knowledge, although there is no evidence for substrate accumulation comparable to that of Gaucher cells in models from *GBA1*-PD patients, we and two previous studies (conducted on iPSC-derived cultures of *GBA1* patients) detected higher levels of GlcCer.[12,55] Moreover, complete inhibition of GCase activity in control MOs treated with CBE also resulted in increased levels of GlcCer and α-synucleinopathy. This finding might be ascribed to the complete loss of enzymatic activity (which does not occur in mutant *GBA1* subjects), but also to other indirect off-target events, either impacting on GCase (one of which is the reduced amount of protein) or α-syn metabolism.

Nonetheless, the increased amount of GlcCer derived from GCase deficiency in *GBA1*-PD is unlikely to be the sole (or even primary) determinant of PD pathology. The similar risk of PD in carriers of one *GBA1* variant, who maintain a variably reduced GCase activity, and in GD patients, displaying a significant loss of enzymatic function, supports the hypothesis that factors other than GCase activity deficit play a role in *GBA1*-PD risk. Moreover, neuropathological studies in old GD subjects without PD did not detect α-syn pathology,[35] whereas specific *GBA1* variants with only a very mild impact on GCase activity (e.g. E326K) are established risk factors of PD.[56] Exploring alternative scenarios to the enzymatic/substrate-centred hypothesis, it has been demonstrated that *GBA1* pathogenic mutations lead to the production of a misfolded GCase protein, which is retained in the ER and activates pathways associated with ER stress.[11,31,57] Mutant GCase undergoes ER-associated degradation, can interfere with chaperone-mediated autophagy and blocks lysosomal degradation of α-syn, thereby promoting α-syn aggregation.[11,31,58] Consistent with this hypothesis, we found that in *GBA1* MOs, mutant GCase was located mainly in the ER and extensively bound to the misfolded protein sensor Grp78, suggesting that most of the protein was retained in a misfolded state. The observation of ER membrane expansion and Grp78-mediated activation of UPR through phosphorylation of the pancreatic-like ER kinase (PERK) downstream effector eIF2α was supportive for ER stress response,[59,60] probably induced by ER accumulation of GCase. Interestingly, control MOs also displayed a low, but still detectable, amount of GCase co-localizing with Grp78 in the absence of ER dilatation. This finding either reproduces the physiological localization of properly folded GCase in the ER during the early stages of its maturation or

Figure 5 Continued
two-way ANOVA with Tukey's *post hoc* test. (**G**) Co-localization percentage of LAMP1 and GCase in PD^{L444P} and GD/PD^{L4444P} MOs at 100 DIV from immunofluorescence images shown in Supplementary Fig. 10C. $n = 3$ biological replicates per line; $^{***}P < 0.001$, $^{**}P < 0.01$, $^{*}P < 0.05$, one-way ANOVA with Dunnett's *post hoc* test. (**H** and **I**) Representative immunofluorescence images of proteinase K (PK)-resistant insoluble α-synuclein (α-syn) immunoreactivity in CTR^{wt}, PD^{L444P} and GD/PD^{L444P} MOs at 100 DIV with and without treatment with AMBR or GZ667161 (**H**), and quantification of α-syn aggregates number per field and relative percentage changes in α-syn area with respect to untreated (**I**). $n = 3$ organoids for each line were analysed by examining an average of five fields per condition from different sections; $^{****}P < 0.0001$, $^{***}P < 0.001$, $^{**}P < 0.01$, $^{*}P < 0.05$, one-way ANOVA with Dunnett's *post hoc* test. Scale bar = 25 µm. In **B**, **D**–**G** and **I**, data are mean ± standard error of the mean. UNTR = untreated.

suggests that a fraction of wild-type GCase requires the activation of Grp78 for efficient folding.

The relevance of these observations is strengthened when coupled to the extensive α-synucleinopathy observed in *GBA1*-PD MOs, given that α-syn aggregation within LBs and LNs is a distinctive neuropathological finding in PD brains. Previous human iPSC-based and brain organoid models did not convincingly recapitulate Lewy pathology. One study showed Thio-T-stained fibrils within TH^+ neurons in CRISPR-engineered isogenic MOs carrying the G2019S *LRRK2* mutation, but no evidence of α-syn fibrils was described.[50] Another study reported on LB-like inclusions in a genetically modified model consisting of midbrain-like organoids derived from human embryonic stem cells in which *GBA1* was knocked out and α-syn overexpressed.[61] A more recent work reported the presence of insoluble and S129 phosphorylated α-syn in *GBA1* mutant organoids.[47] Nevertheless, none of the previous studies demonstrated exhaustively that patient-derived MOs can develop α-syn deposits with the major features of authentic LBs, including decreased solubility, presence of fibrils, reactivity to amyloid-binding dyes, hyperphosphorylation at S129, seeding ability and typical ultrastructural organization. Here, we reported that genetically unmodified MOs from subjects with *GBA1*-related PD developed insoluble α-syn aggregates in the shape of morphologically defined structures mirroring the typical LBs and LNs of PD neuropathology. The observed α-syn immunoreactive deposits ranged from punctate staining to variform compact inclusions, thereby representing diverse stages of the formation process of Lewy aggregates.[62] Moreover, in addition to the presence of insoluble α-syn and of S129 phosphorylated and ubiquitinated α-syn, the localization of Thio-S/α-syn double-positive inclusions in TH^+ neurons in *GBA1*-PD MOs reflected the classical fibrillary organization of α-syn in DA neurons of PD brains. The demonstration that LB-like inclusions in *GBA1* mutant MOs are enriched in crowded organelles and membrane fragments, tubulovesicular structures and aberrantly distributed filaments validates the ability of this model also to mimic closely aspects of the ultrastructural composition of bona fide LB pathology. Strikingly, the similar seeding activity for α-syn displayed by *GBA1*-PD MOs and brain homogenates in the seed amplification assay and upon the injection in healthy MOs supported that the α-syn aggregates/polymorphs from MOs and post-mortem PD brains share similar properties, indicating that this experimental model can appropriately recapitulate key aspects of the pathology of patients.

It is noteworthy that, although we reported marked aggregation of α-syn in both heterozygous and homozygous *GBA1* MOs, we observed an increase in total α-syn content only in the heterozygous PD and not in the GD/PD. One possible explanation could be that the almost complete loss of GCase activity in GD might result in a more pronounced oxidative stress, which, in turn, would enhance α-syn misfolding and aggregation.[63] Consistently, it has been found that α-syn has an increased tendency to form dimers in the erythrocyte membrane of GD patients, and this is related to both the level of lipids, such as GlcCer, and the increased oxidative stress observed in the context of GCase deficiency.[64] Still, the observation that in homozygous *GBA1* MOs total α-syn accumulates selectively in TH^+ neurons supports the relevance of this model to recapitulate fundamental pathological events in PD and warrants further studies to investigate the multiplicity of mechanisms behind α-syn pathology.

An additional question that our study tried to address pertains the temporal relationship between GCase defects and α-synucleinopathy. In the heterozygous and homozygous *GBA1* mutant MOs, the initial accumulation of α-syn within TH^+ neurons, which is seemingly the first step of the aggregation process, occurred at the same stage (i.e. 50 DIV). However, the fact that the GlcCer amount was normal in the heterozygous MOs at 65 DIV suggested that substrate content, which reflects the residual GCase activity, did not play an initiating role in α-syn pathology. Likewise, the observation of Lewy-like inclusions at an earlier time point than GlcCer increase in the monoallelic *GBA1*-PD^{L444P} MOs supports this hypothesis. This having been established, the earlier conversion of α-syn into insoluble forms in GD/PD^{L444P} (i.e. 60 DIV) compared with PD^{L444P} (i.e. 80 DIV) suggested a more rapid progression of PD pathology. This could be explained by the earlier increase in the amount of GlcCer, which might act as a modulating factor in the dynamics of α-syn pathology, in line with recent observations in models of GCase inhibition.[54] Interestingly, the levels of Syn III, a presynaptic phosphoprotein found in LBs and implicated in α-syn aggregation,[14,40,41] also increased earlier in GD/PD^{L444P} MOs, supporting an accelerated aggregation process.

Finally, we investigated the potential of MOs as a patient-derived model for the screening of candidate therapeutic compounds. Although enzyme replacement therapy and substrate reduction therapy are approved treatments to address GCase insufficiency in GD, there is no specific therapy for *GBA1*-related PD. Tackling impaired GCase metabolism to act on downstream effects of α-syn accumulation is a rapidly expanding avenue of research in drug development for PD. Molecules engaging with the GCase pathway have entered clinical trials for PD, including the open-label clinical trial testing ambroxol[65] (NCT02941822) and the phase II trial on the GlcCer synthase inhibitor venglustat[66] (NCT02906020). The observations of mutated GCase undergoing aberrant post-translational folding increasingly clarify the mechanism by which ER-retained GCase induces UPR and α-syn aggregation.[11] In this respect, ambroxol might modulate α-syn pathology by assisting the correct folding of GCase in the ER and facilitating its trafficking to the lysosome.[32] In our study, ambroxol proved to increase the levels of GCase protein in MOs of both *GBA1*-mutated patients, to improve the trafficking of the enzyme to its physiological lysosomal location and to reduce the load of Lewy-like pathology significantly. Notably, the observation that ambroxol-treated GD/PD^{L444P} MOs did not increase GCase activity and that GlcCer levels were not affected in *GBA1* mutants suggested that the rescue of α-syn aggregates was not directly linked to the function of the enzyme. Moreover, even when GCase activity was restored, as observed in the heterozygous *GBA1* MO, GlcCer levels remained higher than in wild-type MOs, suggesting either that ambroxol directs GCase partly to non-lysosomal compartments or that GlcCer also accumulates in membrane domains other than the lysosome.[67]

Exploring the hypothesis of GlcCer accumulation as a major player in α-syn pathology, we also tested the GlcCer synthase inhibitor GZ667161, which completely suppressed new production of GlcCer in MOs. Notably, treatment with GZ667161 markedly attenuated Lewy-like pathology, in line with previous observations in GD and PD mouse models.[43] Levels of total α-syn, unlike the aggregated form, were not affected by exposure to GZ667161. This observation suggested that GlcCer favours the conversion of physiological α-syn to its insoluble form, while the reduction in the amount of GlcCer shifts the soluble–insoluble α-syn balance towards its physiological, soluble form. Therefore, GZ667161 appears efficiently to overcome one of the main limitations associated with α-syn clearing strategies, which is the development of a possible soluble 'α-synucleinopenia'.[68] Interestingly, Syn III, which co-aggregates with α-syn in LB fibrils, was also reduced by the treatment. One possible explanation might imply a GlcCer-dependent remodelling of membranes, which could prevent the formation of new aggregates and, by favouring soluble α-syn increase, allow a more efficient dispersion of synaptic vesicles, with which Syn III interacts.[69] The

reciprocal regulation of α-syn and Syn III in synaptic vesicle release is sustained by findings showing that Syn III is low in wild-type mice with physiological levels of soluble α-syn, whereas α-syn null mice, similar to animals that by developing pathological α-syn aggregates display a loss of function of soluble α-syn, exhibit increased Syn III accumulation and synaptic vesicle clumping.[40,41,69] Alternatively, by favouring the degradation of Syn III, which acts as an α-syn fibril stabilizer, GZ667161 leads to a reduction of fibrils, thus reproducing the same α-syn pathology rescue observed following *in vivo* Syn III gene silencing in transgenic mice.[70] However, the precise mechanism by which GlcCer synthase inhibition results in the attenuation of α-syn pathology demands further investigation. Likewise, we need to deepen the significance of GCase retention within the ER and its impact on α-syn pathology.

Lastly, the potential of ambroxol and GZ667161 to have an impact on the survival of neurons in PD remains an essential point to be clarified. Although our results support the use of ambroxol in the heterozygous *GBA1*-PD for improved neuronal survival, our experiments with ambroxol in GD/PD and with GZ667161 did not meet this end point and agree with recent results on the effect of venglustat in *GBA1*-mutated mice overexpressing human α-syn.[71] Our data support that, although ambroxol and GZ667161 are both able to reduce α-syn pathology significantly, the different effect exerted by these compounds on GCase levels and activity, either increased by ambroxol or not as in the case of GZ667161, might underlie their diverse impact on neuronal survival. It should also be pointed out that in our study drug testing was carried out when neurodegeneration had already been established (i.e. at 100 DIV) and it could be speculated that an earlier timing for pharmacological intervention might instead have exerted a neuroprotective effect.

Conclusion

In conclusion, we present an innovative MO-based culture system derived from patients with *GBA1*-PD capable of reproducing key features of Lewy pathology and neurodegeneration. The concomitant occurrence of α-synucleinopathy in monoallelic and biallelic *GBA1* MOs suggests a shared common initiating event for both, probably misfolded mutant GCase retained in the ER. Still, the severity of GCase activity reduction and Syn III increase might act as accelerating factors in the progression of α-syn pathology by favouring the conversion of soluble α-syn to its insoluble forms. Finally, the observation of α-syn pathology rescue with ambroxol and GZ667161, which act at different levels of the GCase pathway, endorses the use of MOs as a patient-specific tool for a broader implementation of personalized medicine.

Data availability

RNA-seq data are deposited in the Zenodo repository (https://doi.org/10.5281/zenodo.5607334) with restricted access and are available on request. The data are not publicly available because they contain information that could compromise research participant consent and privacy. Requests to access the data should be sent to biblioteca@humanitas.it.

Acknowledgements

We thank M. Brevi, G. Alfonsi, E. Bistaffa, M. Pannella, G. Pires and the NYU Center for Biospecimen Research and Development for processing of specimens; and F. Carubbi and F. Nascimbeni of the University of Modena and Reggio Emilia for providing clinical and biological material. We also acknowledge ALEMBIC (Advanced Light and Electron Microscopy BioImaging Center) at IRCCS Ospedale San Raffaele for EM analyses; Euro-BioImaging (www.eurobioimaging.eu) for providing access to imaging technologies and services via the Italian Node (ALEMBIC, Milan, Italy). The authors would like to acknowledge Fresco Institute for Parkinson's and Movement Disorders and the Dino Ferrari Center for support. The authors warmly remember co-investigators Professor Stefano Duga (16 September 1967–10 November 2021), geneticist, and Professor Nereo Bresolin (25 August 1952–2 May 2023), neurologist, for their enthusiasm and inspiration over the years.

Funding

Ministero dell'Università e della Ricerca 2017228L3J (R.A., M.A. and M.B.); Ministero della Salute Ricerca Corrente (A.D.F. and F.M.); Fondazione Cariplo 2015–1017 (M.A.); Ministero della Salute GR-2021-12372019 (F.M.); Ministero della Salute PNRR-MAD-2022-12376035 (F.M.); National Institutes of Health/National Institute of Aging P30AG066512 (T.W.); National Institutes of Health/National Institute of Aging P01AG060882 (T.W.); Fondazione Grigioni per il Morbo di Parkinson (L.S.); Fondazione Regionale per la Ricerca Biomedica 825575 (A.D.F.); Mizutani Foundation for Glycoscience 220054 (M.A.).

Competing interests

The authors report no competing interests. S.P.S. is an employee and stockholder of Sanofi. He provided the molecule GZ667161 that was tested in midbrain organoids. To avoid potential biases, this author was excluded from experiments and analysis of data concerning use of GZ667161 in midbrain organoids. No research funding was obtained from any company for the present study.

Supplementary material

Supplementary material is available at *Brain* online.

References

1. Feigin VL, Nichols E, Alam T, et al. Global, regional, and national burden of neurological disorders, 1990–2016: A systematic analysis for the global burden of disease study 2016. *Lancet Neurol*. 2019;18:459-480.
2. GBD 2016 Parkinson's Disease Collaborators. Global, regional, and national burden of Parkinson's disease, 1990–2016: a systematic analysis for the Global Burden of Disease Study 2016 [published correction appears in Lancet Neurol. 2021;20:e7.]. *Lancet Neurol*. 2018;17:939-953.
3. Goedert M, Spillantini MG, Del Tredici K, Braak H. 100 years of Lewy pathology. *Nat Rev Neurol*. 2013;9:13-24.
4. Spillantini MG, Schmidt ML, Lee VM, Trojanowski JQ, Jakes R, Goedert M. α-Synuclein in Lewy bodies. *Nature*. 1997;388:839-840.
5. Shahmoradian SH, Lewis AJ, Genoud C, et al. Lewy pathology in Parkinson's disease consists of crowded organelles and lipid membranes. *Nat Neurosci*. 2019;22:1099-1109.

6. Fares MB, Jagannath S, Lashuel HA. Reverse engineering Lewy bodies: How far have we come and how far can we go? *Nat Rev Neurosci*. 2021;22:111-131.
7. Sidransky E, Nalls MA, Aasly JO, et al. Multicenter analysis of glucocerebrosidase mutations in Parkinson's disease. *N Engl J Med*. 2009;361:1651-1661.
8. Grabowski GA. Phenotype, diagnosis, and treatment of Gaucher's disease. *Lancet*. 2008;372:1263-1271.
9. Riboldi GM, Di Fonzo AB. *GBA*, Gaucher disease, and Parkinson's disease: From genetic to clinic to new therapeutic approaches. *Cells*. 2019;8:364.
10. Mazzulli JR, Xu YH, Sun Y, et al. Gaucher disease glucocerebrosidase and α-synuclein form a bidirectional pathogenic loop in synucleinopathies. *Cell*. 2011;146:37-52.
11. Maor G, Rencus-Lazar S, Filocamo M, Steller H, Segal D, Horowitz M. Unfolded protein response in Gaucher disease: From human to *Drosophila*. *Orphanet J Rare Dis*. 2013;8:140.
12. Schöndorf DC, Aureli M, McAllister FE, et al. iPSC-derived neurons from GBA1-associated Parkinson's disease patients show autophagic defects and impaired calcium homeostasis. *Nat Commun*. 2014;5:4028.
13. Smith L, Schapira AHV. *GBA* variants and Parkinson disease: Mechanisms and treatments. *Cells*. 2022;11:1261.
14. Longhena F, Faustini G, Varanita T, et al. Synapsin III is a key component of α-synuclein fibrils in Lewy bodies of PD brains. *Brain Pathol*. 2018;28:875-888.
15. Lancaster MA, Knoblich JA. Generation of cerebral organoids from human pluripotent stem cells. *Nat Protoc*. 2014;9: 2329-2340.
16. Kriks S, Shim JW, Piao J, et al. Dopamine neurons derived from human ES cells efficiently engraft in animal models of Parkinson's disease. *Nature*. 2011;480:547-551.
17. Drummond E, Nayak S, Ueberheide B, Wisniewski T. Localized proteomics of individual neurons isolated from formalin-fixed, paraffin-embedded tissue sections using laser capture microdissection. In: Santamaría E, Fernández-Irigoyen J, eds. *Current proteomic approaches applied to brain function. Neuromethods*. Vol 127. Humana Press; 2017:289-301.
18. Drummond E, Nayak S, Pires G, Ueberheide B, Wisniewski T. Isolation of amyloid plaques and neurofibrillary tangles from archived Alzheimer's disease tissue using laser-capture microdissection for downstream proteomics. *Methods Mol Biol*. 2018; 1723:319-334.
19. McKenzie AT, Wang M, Hauberg ME, et al. Brain cell type specific gene expression and co-expression network architectures. *Sci Rep*. 2018;8:8868.
20. Sloan SA, Darmanis S, Huber N, et al. Human astrocyte maturation captured in 3D cerebral cortical spheroids derived from pluripotent stem cells. *Neuron*. 2017;95:779-790.e6.
21. Poulin JF, Zou J, Drouin-Ouellet J, Kim KYA, Cicchetti F, Awatramani RB. Defining midbrain dopaminergic neuron diversity by single-cell gene expression profiling. *Cell Rep*. 2014;9: 930-943.
22. Svennerholm L, Boström K, Fredman P, Månsson JE, Rosengren B, Rynmark BM. Human brain gangliosides: Developmental changes from early fetal stage to advanced age. *Biochim Biophys Acta*. 1989;1005:109-117.
23. Zecca L, Bellei C, Costi P, et al. New melanic pigments in the human brain that accumulate in aging and block environmental toxic metals. *Proc Natl Acad Sci U S A*. 2008;105:17567-17572.
24. Moses HL, Ganote CE, Beaver DL, Schuffman SS. Light and electron microscopic studies of pigment in human and rhesus monkey substantia nigra and locus coeruleus. *Anat Rec*. 1966;155:167-183.
25. Gegg ME, Burke D, Heales SJR, et al. Glucocerebrosidase deficiency in substantia nigra of Parkinson disease brains. *Ann Neurol*. 2012;72:455-463.
26. Parnetti L, Chiasserini D, Persichetti E, et al. Cerebrospinal fluid lysosomal enzymes and alpha-synuclein in Parkinson's disease. *Mov Disord*. 2014;29:1019-1027.
27. Huebecker M, Moloney EB, van der Spoel AC, et al. Reduced sphingolipid hydrolase activities, substrate accumulation and ganglioside decline in Parkinson's disease. *Mol Neurodegener*. 2019;14:40.
28. Gegg ME, Sweet L, Wang BH, Shihabuddin LS, Sardi SP, Schapira AHV. No evidence for substrate accumulation in Parkinson brains with *GBA* mutations. *Mov Disord*. 2015;30:1085-1089.
29. Boutin M, Sun Y, Shacka JJ, Auray-Blais C. Tandem mass spectrometry multiplex analysis of glucosylceramide and galactosylceramide isoforms in brain tissues at different stages of Parkinson disease. *Anal Chem*. 2016;88:1856-1863.
30. Leyns CEG, Prigent A, Beezhold B, et al. Glucocerebrosidase activity and lipid levels are related to protein pathologies in Parkinson's disease. *NPJ Park Dis*. 2023;9:74.
31. Ron I, Horowitz M. ER retention and degradation as the molecular basis underlying Gaucher disease heterogeneity. *Hum Mol Genet*. 2005;14:2387-2398.
32. Bendikov-Bar I, Ron I, Filocamo M, Horowitz M. Characterization of the ERAD process of the L444P mutant glucocerebrosidase variant. *Blood Cells Mol Dis*. 2011;46:4-10.
33. Hetz C. The unfolded protein response: Controlling cell fate decisions under ER stress and beyond. *Nat Rev Mol Cell Biol*. 2012;13: 89-102.
34. Tayebi N, Walker J, Stubblefield B, et al. Gaucher disease with parkinsonian manifestations: Does glucocerebrosidase deficiency contribute to a vulnerability to parkinsonism? *Mol Genet Metab*. 2003;79:104-109.
35. Wong K, Sidransky E, Verma A, et al. Neuropathology provides clues to the pathophysiology of Gaucher disease. *Mol Genet Metab*. 2004;82:192-207.
36. Fujiwara H, Hasegawa M, Dohmae N, et al. α-Synuclein is phosphorylated in synucleinopathy lesions. *Nat Cell Biol*. 2002;4: 160-164.
37. Anderson JP, Walker DE, Goldstein JM, et al. Phosphorylation of Ser-129 is the dominant pathological modification of α-synuclein in familial and sporadic Lewy body disease. *J Biol Chem*. 2006;281:29739-29752.
38. Kuzuhara S, Mori H, Izumiyama N, Yoshimura M, Ihara Y. Lewy bodies are ubiquitinated. A light and electron microscopic immunocytochemical study. *Acta Neuropathol*. 1988;75:345-353.
39. Henderson MX, Cornblath EJ, Darwich A, et al. Spread of α-synuclein pathology through the brain connectome is modulated by selective vulnerability and predicted by network analysis. *Nat Neurosci*. 2019;22:1248-1257.
40. Faustini G, Longhena F, Varanita T, et al. Synapsin III deficiency hampers α-synuclein aggregation, striatal synaptic damage and nigral cell loss in an AAV-based mouse model of Parkinson's disease. *Acta Neuropathol*. 2018;136:621-639.
41. Faustini G, Longhena F, Bruno A, et al. Alpha-synuclein/synapsin III pathological interplay boosts the motor response to methylphenidate. *Neurobiol Dis*. 2020;138:104789.
42. Magalhaes J, Gegg ME, Migdalska-Richards A, Schapira AH. Effects of ambroxol on the autophagy-lysosome pathway and mitochondria in primary cortical neurons. *Sci Rep*. 2018;8:1385.
43. Sardi SP, Viel C, Clarke J, et al. Glucosylceramide synthase inhibition alleviates aberrations in synucleinopathy models. *Proc Natl Acad Sci U S A*. 2017;114:2699-2704.

44. Jo J, Xiao Y, Sun AX, et al. Midbrain-like organoids from human pluripotent stem cells contain functional dopaminergic and neuromelanin-producing neurons. *Cell Stem Cell*. 2016;19:248-257.
45. Monzel AS, Smits LM, Hemmer K, et al. Derivation of human midbrain-specific organoids from neuroepithelial stem cells. *Stem Cell Rep*. 2017;8:1144-1154.
46. Fiorenzano A, Sozzi E, Birtele M, et al. Single-cell transcriptomics captures features of human midbrain development and dopamine neuron diversity in brain organoids. *Nat Commun*. 2021;12:7302.
47. Baden P, Perez MJ, Raji H, et al. Glucocerebrosidase is imported into mitochondria and preserves complex I integrity and energy metabolism. *Nat Commun*. 2023;14:1930.
48. Reumann D, Krauditsch C, Novatchkova M, et al. In vitro modeling of the human dopaminergic system using spatially arranged ventral midbrain–striatum–cortex assembloids. *Nat Methods*. 2023;20:2034-2047.
49. Galet B, Cheval H, Ravassard P. Patient-derived midbrain organoids to explore the molecular basis of Parkinson's disease. *Front Neurol*. 2020;11:1005.
50. Kim H, Park HJ, Choi H, et al. Modeling G2019S-LRRK2 sporadic Parkinson's disease in 3D midbrain organoids. *Stem Cell Rep*. 2019;12:518-531.
51. Kwak TH, Kang JH, Hali S, et al. Generation of homogeneous midbrain organoids with in vivo-like cellular composition facilitates neurotoxin-based Parkinson's disease modeling. *Stem Cells*. 2020;38:727-740.
52. Smits LM, Reinhardt L, Reinhardt P, et al. Modeling Parkinson's disease in midbrain-like organoids. *NPJ Park Dis*. 2019;5:5.
53. Tribl F, Arzberger T, Riederer P, Gerlach M. Tyrosinase is not detected in human catecholaminergic neurons by immunohistochemistry and western blot analysis. *J Neural Transm Suppl*. 2007;72:51-55.
54. Henderson MX, Sedor S, McGeary I, et al. Glucocerebrosidase activity modulates neuronal susceptibility to pathological α-synuclein insult. *Neuron*. 2020;105:822-836.e7.
55. Burbulla LF, Jeon S, Zheng J, Song P, Silverman RB, Krainc D. A modulator of wild-type glucocerebrosidase improves pathogenic phenotypes in dopaminergic neuronal models of Parkinson's disease. *Sci Transl Med*. 2019;11:eaau6870.
56. Horowitz M, Pasmanik-Chor M, Ron I, Kolodny EH. The enigma of the E326K mutation in acid β-glucocerebrosidase. *Mol Genet Metab*. 2011;104:35-38.
57. Fernandes HJR, Hartfield EM, Christian HC, et al. ER stress and autophagic perturbations lead to elevated extracellular α-synuclein in GBA-N370S Parkinson's iPSC-derived dopamine neurons. *Stem Cell Rep*. 2016;6:342-356.
58. Kuo SH, Tasset I, Cheng MM, et al. Mutant glucocerebrosidase impairs α-synuclein degradation by blockade of chaperone-mediated autophagy. *Sci Adv*. 2022;8:eabm6393.
59. Oslowski CM, Urano F. Measuring ER stress and the unfolded protein response using mammalian tissue culture system. *Methods Enzymol*. 2011;490:71-92.
60. Bellucci A, Navarria L, Zaltieri M, et al. Induction of the unfolded protein response by α-synuclein in experimental models of Parkinson's disease: α-synuclein accumulation induces the UPR. *J Neurochem*. 2011;116:588-605.
61. Jo J, Yang L, Tran HD, et al. Lewy body-like inclusions in human midbrain organoids carrying glucocerebrosidase and α-synuclein mutations. *Ann Neurol*. 2021;90:490-505.
62. Kuusisto E, Parkkinen L, Alafuzoff I. Morphogenesis of Lewy bodies: Dissimilar incorporation of α-synuclein, ubiquitin, and p62. *J Neuropathol Exp Neurol*. 2003;62:1241-1253.
63. Scudamore O, Ciossek T. Increased oxidative stress exacerbates α-synuclein aggregation in vivo. *J Neuropathol Exp Neurol*. 2018;77:443-453.
64. Moraitou M, Dermentzaki G, Dimitriou E, et al. α-Synuclein dimerization in erythrocytes of Gaucher disease patients: Correlation with lipid abnormalities and oxidative stress. *Neurosci Lett*. 2016;613:1-5.
65. Mullin S, Smith L, Lee K, et al. Ambroxol for the treatment of patients with Parkinson disease with and without glucocerebrosidase gene mutations: A nonrandomized, noncontrolled trial. *JAMA Neurol*. 2020;77:427-434.
66. Giladi N, Alcalay RN, Cutter G, et al. Safety and efficacy of venglustat in *GBA1*-associated Parkinson's disease: An international, multicentre, double-blind, randomised, placebo-controlled, phase 2 trial. *Lancet Neurol*. 2023;22:661-671.
67. Lunghi G, Carsana EV, Loberto N, et al. β-Glucocerebrosidase deficiency activates an aberrant lysosome-plasma membrane axis responsible for the onset of neurodegeneration. *Cells*. 2022;11:2343.
68. Espay AJ, McFarthing K. Alpha-synuclein and the Parkinson's disease drug pipeline. *Parkinsonism Relat Disord*. 2023;111:105432.
69. Zaltieri M, Grigoletto J, Longhena F, et al. α-Synuclein and synapsin III cooperatively regulate synaptic function in dopamine neurons. *J Cell Sci*. 2015;128:2231-2243.
70. Faustini G, Longhena F, Masato A, et al. Synapsin III gene silencing redeems alpha-synuclein transgenic mice from Parkinson's disease-like phenotype. *Mol Ther*. 2022;30:1465-1483.
71. Schidlitzki A, Stanojlovic M, Fournier C, et al. Double-edged effects of venglustat on behavior and pathology in mice overexpressing α-synuclein. *Mov Disord*. 2023;38:1044-1055.